Marine Chemistry xxx (xxxx) xxx–xxx

Contents lists available at ScienceDirect

Marine Chemistry

journal homepage: www.elsevier.com/locate/marchem

Cobalt scavenging in the mesopelagic ocean and its influence on global mass balance: Synthesizing water column and sedimentary fluxes

Nicholas J. Hawco[a,b], Phoebe J. Lam[c], Jong-Mi Lee[c], Daniel C. Ohnemus[d], Abigail E. Noble[e], Neil J. Wyatt[f], Maeve C. Lohan[f], Mak A. Saito[b,*]

[a] MIT/WHOI Joint Program in Oceanography/Applied Ocean Science and Engineering, Woods Hole, MA, USA
[b] Department of Marine Chemistry and Geochemistry, Woods Hole Oceanographic Institution, Woods Hole, MA, USA
[c] Department of Ocean Sciences, University of California Santa Cruz, Santa Cruz, CA, USA
[d] Bigelow Laboratory for Ocean Sciences, East Boothbay, ME, USA
[e] Gradient, 20 University Road, Cambridge, MA, USA
[f] School of Ocean and Earth Sciences, National Oceanography Centre, University of Southampton, Southampton, UK

ARTICLE INFO

Keywords:
Constant flux chronometer
Residence times
Remineralization
GEOTRACES

ABSTRACT

In the ocean, dissolved cobalt is affected by both nutrient cycling and scavenging onto manganese oxides. The latter process concentrates Co in pelagic sediments, resulting in a small deep water inventory. While the flux of scavenged cobalt to sediments appears steady on timescales > 100,000 years, its residence time in the water column is short, approximately 130 years. Using results from recent GEOTRACES expeditions, we show net removal of dissolved Co from the deep ocean on the order of 0.043 pM $year^{-1}$, which corresponds to a turnover time of 980 years. Scavenging in deep ocean water masses is too slow to match cobalt accumulation rates in marine sediments, requiring most of the scavenging flux to derive from the mesopelagic ocean (< 1500 m depth) where nutrient cycling is active. Based on differences between the Co:P stoichiometry in particles sinking from the euphotic zone and dissolved Co:P remineralization ratios, we calculate areal scavenging rates in the North Atlantic and South Pacific basins on the order of 1.5 and 0.7 μmol m^{-2} $year^{-1}$, respectively, which agree with long-term accumulation rates in Atlantic and Pacific sediments. In both basins, over 50% of the scavenged flux of cobalt occurs in the upper 500 m, resulting in decadal turnover times in the mesopelagic. An assessment of sources suggests that the marine cobalt cycle is approximately in balance, but that this inventory may be sensitive to long term trends in the intensity of oxygen minimum zones, which account for ~25% of the annual cobalt source to the modern oceans.

1. Introduction

In pelagic sediments, cobalt is enriched over its crustal sources – shale, basalts, andesites – sometimes to a factor of 10 or higher (Goldberg and Arrhenius, 1958; Krishnaswami, 1976). This excess can be attributed to scavenging reactions occurring in the water column that incorporate cobalt into authigenic manganese oxides that then sink from the water column (Cowen and Bruland, 1985; Moffett and Ho, 1996). Manganese nodules and crusts can be appreciated as the extreme of this enrichment, where Co concentrations can be several percent by mass in extremely slow growing specimens (Manheim, 1986). On long time scales, the flux of Co to marine sediments and nodules is steady, an observation that has been exploited to improve sedimentary age models when other dating techniques are unavailable (Dunlea et al., 2015; Halbach et al., 1983; Krishnaswami, 1976). Yet an oceanographic explanation of this phenomenon is lacking. Radiotracer and microscopic evidence support a bacterial basis for Mn-oxide production in the upper water column but Mn-oxides produced near the ocean surface are also subject to light-driven dissolution, resulting in a small residual that actually gets exported to the ocean floor and making these results difficult to apply at scale (Cowen and Bruland, 1985; Moffett and Ho, 1996; Sunda and Huntsman, 1988).

In the upper water column, however, cobalt cycling is dominated by its role as a nutrient. Cobalt is important for phytoplankton CO_2 fixation via the metalloenzyme carbonic anhydrase and, as the central atom in vitamin B_{12}, cobalt is also required by many organisms for the biosynthesis of DNA and the amino acid methionine (Yee and Morel, 1996; Zhang et al., 2009). From these biochemical roles, low concentrations of cobalt in the surface ocean have the potential to limit marine productivity, though it is not clear if this is widespread in the modern

* Corresponding author at: 266 Woods Hole Road MS#51, Woods Hole, MA 02543, USA.
E-mail address: msaito@whoi.edu (M.A. Saito).

http://dx.doi.org/10.1016/j.marchem.2017.09.001
Received 27 March 2017; Received in revised form 2 August 2017; Accepted 1 September 2017

ocean (Moore et al., 2013; Saito et al., 2005). Profiles of dissolved cobalt, dCo, are strongly impacted by biological uptake and regeneration, resulting in strong correlations with phosphate in the upper water column (Saito and Moffett, 2002; Saito et al., 2010). Remineralization also contributes to elevated dCo within oxygen minimum zones in both the Atlantic and Pacific Oceans (Hawco et al., 2016; Noble et al., 2017, 2012). In deeper waters, however, dCo and PO_4 decouple as dCo is removed from the water column by scavenging, yet the exact locus or horizon where scavenging occurs is difficult to discern due to the combined effects of circulation and remineralization (Dulaquais et al., 2014b; Saito et al., 2010).

Here, we trace dCo removal by scavenging throughout the global ocean by synthesizing thousands of recent water column measurements with Co accumulation rates in sediments and rates of supply from continents. Our calculations portray a fast and perturbable Co cycle that make its apparent steadiness on > 100,000 year timescales all the more surprising.

2. Methods

Drastic differences in timescales associated with upper ocean (< 1500 m), deep ocean (> 1500 m), and sedimentary processes preclude the application of a single tracer/method to estimate scavenging fluxes for each of these environments. Accordingly, we have approached these strata separately. Global extrapolations of cobalt scavenging are based on sedimentary accumulation rates and provide a view of the cobalt cycle on timescales of 100,000 years or greater. The millennial ventilation age of the deep ocean enables comparison with the radiocarbon content of dissolved inorganic carbon to 'clock' the loss of cobalt from these waters, while the faster ventilation of overlying waters requires comparison with particulate cobalt datasets and consideration of the magnitudes of biological cobalt export from the euphotic zone (0–100 m depth) and its remineralization in the mesopelagic zone (defined here as here 100–1500 m).

2.1. Global cobalt cycle calculations

Average dissolved cobalt was defined as the median of the datasets included in Fig. S1 (n = 2920), 46 pM, which is similar to values used in previous residence time calculations (Saito and Moffett, 2002). Ocean volumes and surface areas from the ETOPO1 dataset are used (Eakins and Sharman, 2010). In estimating global cobalt sinks, a paucity of data requires extrapolation of a small number of sedimentary fluxes in Table 1 to large areas. This estimate is aided by the observation that the flux of excess cobalt to marine sediments has a relatively constant spatial distribution (See Results and Discussion; Goldberg and Arrhenius, 1958; Kadko, 1985; Krishnaswami, 1976), and from the fact that the largest two basins – the Pacific and Atlantic – are also the best characterized. Because circulation in the Arctic and Mediterranean basins is restricted, they have been excluded from global calculations. We are not aware of measurements of cobalt accumulation rates in Indian and Southern Ocean sediments, which compose the remaining 30% of ocean surface area, and have extrapolated Quaternary Pacific Ocean averages (Table 1, ~1.1 μmol m^{-2} $year^{-1}$) for these basins, which are lower than areal fluxes from the Atlantic (~1.9 μmol m^{-2} $year^{-1}$) and therefore reflect a more conservative estimate. These estimates should be updated as new data becomes available. For the time being, we use maximum and minimum sedimentary fluxes to establish upper and lower limits for this global sink of cobalt.

For lithogenic/detrital corrections to marine sediments and sinking particles (see below), we have used a uniform Co:Ti ratio of upper continental crust (3.37×10^{-3} mol mol^{-1}) defined by McLennan (2001). If Ti concentration was not available, a value of 17 ppm was used to estimate detrital Co composition (McLennan, 2001). This approach assumes dissolution of aerosol cobalt is low. The 8–10% dissolution of cobalt from Saharan aerosols (Shelley et al., 2012) suggests that the above Ti-corrections are appropriate but might underestimate co-occurring biogenic and authigenic phases when lithogenic contributions are high (e.g. the North Atlantic).

Table 1
Literature estimates of the non-detrital cobalt flux to marine sediments (K).

Location	Non-detrital Co flux μmol m^{-2} $year^{-1}$	Source
Mn crusts and nodules		
Central Pacific	0.40	Halbach et al., 1983 and Dunlea et al., 2015
Atlantic, Pacific and Indian	0.32	Frank et al., 1999
Pacific sediments, Cenozoic		
North Pacific Gyre	0.44 ± 0.07	Kyte et al., 1993
South Pacific Gyre	0.34 ± 0.06	Dunlea et al., 2015
South Pacific Gyre	0.34	Zhao and Kyte, 1992
Pacific sediments, Quaternary		
Pacific surface sediments	0.93[a]	Krishnaswami, 1976
North Pacific Gyre	1.16	Kyte et al., 1993
Northeast Pacific	1.2[b]	Kadko, 1985
South Pacific Gyre	1.2	Windom, 1970
Atlantic sediments, Quaternary		
Sargasso sea	2.3 ± 0.4	Thomson et al., 1984
Sargasso sea	1.2 ± 1.0	Bacon and Rosholt, 1982
Hatteras continental rise	2.5 (2–3)	Heggie and Lewis, 1984
South Atlantic Gyre	1.6 ± 0.7[b]	Turekian, 1968
Bermuda sediment traps, 3000 m	2.3 ± 0.1[a]	Huang and Conte, 2009

[a] Modified from published estimates using Ti and the molar Co:Ti ratio of upper continental crust (3.37×10^{-3}, McLennan, 2001).
[b] Modified for a detrital Co concentration matching updated values of Co in upper continental crust (17 ppm, McLennan, 2001).

2.2. Radiocarbon data matching procedure

The net rate of dissolved cobalt (dCo) scavenging in the deep ocean was calculated by comparison with the radiocarbon age of deep ocean waters by both 1) determining basin averages and 2) pairing individual samples collected at the same depth and location. Dissolved cobalt datasets for GA03, GA10, GP16, GIPY4, GAc01 (also known as CoFeMUG), and GPc03 (also known as METZYME) transects were accessed from the literature and data repositories (Table 2, Fig. S1). These datasets were generated either by voltammetry or flow-injection methods following UV-oxidation and authors report measurements of seawater standards that agree with community consensus values (Bown et al., 2011; Hawco et al., 2016; Noble et al., 2017, 2012; Wyatt and Lohan, unpublished; Hawco and Saito, unpublished;). Each of these datasets have been included in the GEOTRACES Intermediate Data Product (IDP) 2017 and are available for download from the GEOTRACES website (www.geotraces.org/dp/intermediate-data-product-2017) and can also be accessed individually on BCO-DMO or BODC. Quality-controlled measurements of the radiocarbon content of dissolved inorganic carbon ($\Delta^{14}C$) in the GLODAP database were downloaded (http://cdiac.ornl.gov/oceans/glodap/; Key et al., 2004).

For basin averages, stations containing $\Delta^{14}C$ data were matched to individual GEOTRACES sections by defining a rectangle whose dimensions were extended 5° latitude and longitude from the maximum extent of the GEOTRACES sections (Table 2, Fig. S1; Key et al., 2004). $\Delta^{14}C$ and dCo datasets were then sorted into an upper bathypelagic bin (in practice 1490–2990 m) and a bottom-water bin (> 2990 m). Because $\Delta^{14}C$ contains a variable amount of anthropogenic radiocarbon produced from nuclear weapons testing, pre-bomb $\Delta^{14}C$ (Nat14C) from GLODAP were used to calculate age, according to the equation:

Table 2
$\Delta^{14}C$ and dCo comparison averaged across domains for GEOTRACES transects.

	Dataset	Box dimensions GEOTRACES/GLODAP	Depth range km	Box averages					
		[N,S,E,W]		$\Delta^{14}C$	σ	n	dCo	σ	n
Atlantic	GA03	[40,17,-10,-70]/	1.5–3	− 84	9	253	73.7	9.9	133
		[44,12,-10,-74]	> 3	− 101	11	288	53.2	10.8	93
	GAc01	[− 11,-25,13,-30]/	1.5–3	− 105	11	103	72.1	17.2	41
		[− 6,-30,9,-35]	> 3	− 139	26	136	50.9	12.2	37
	GA10	[− 34,-40,17,-52]/	1.5–3	− 121	11	109	52.5	5.4	118
		[− 29,-45,19,-51]	> 3	− 152	26	136	36.6	7.4	130
Southern Ocean	GIPY4	[− 34,-58,0,-14]/	1.5–3	− 128	12	75	43.4	7.8	25
		[− 29,-55,2.3,-19]	> 3	− 143	15	90	37.6	7.1	11
Pacific	GP16	[− 10,-16,-78,-152]/	1.5–3	− 198	12	101	31.1	6.6	230
		[− 6,-20,-85,-151]	> 3	− 204	11	78	24.7	4.5	114
	GPc3	[17,-15,-154,-175]/	1.5–3	− 208	15	61	26.8	6.2	48
		[18,-17,150,179]	> 3	− 205	13	88	24.7	4.1	42

$$\text{Age} = -8033 \times \ln(1 + 0.001 \times (\Delta^{14}C + 67)) \quad (1)$$

which subtracts the 'preformed' value of $\Delta^{14}C$ of North Atlantic Waters, − 67‰ (Matsumoto, 2007). This corresponds to the 'Natural' radiocarbon age, which is not reset during ventilation in the Southern Ocean due to very long equilibration times of $\Delta^{14}C$ with the atmosphere. The 'Real' $\Delta^{14}C$ age, which accounts for this effect by determining the fraction of North Atlantic Deep water (NADW) vs. Antarctic Bottom waters (AABW) using the P* tracer ($P^* = PO_4 + \frac{1}{175}O_2 - 1.95$), was also investigated (Fig. S2). An endmember value of P^* of 0.73 μM was applied to NADW and 1.95 μM was applied to AABW (Matsumoto, 2007). Preformed $\Delta^{14}C$ for calculating the 'Real' $\Delta^{14}C$ is then calculated based on the fraction of NADW and AABW (endmember values of − 67‰ and − 140‰, respectively), and added to the exponent in Eq. (1) (Fig. S2).

In addition to basin averages, discreet pairing of individual $\Delta^{14}C$ and dCo measurements was accomplished by matching GLODAP stations containing $\Delta^{14}C$ and dCo stations. Stations within a 5° radius were matched and, in the case of multiple stations, minimum distance was used to determine the closest station. For each transect, no dCo station is matched to more than one $\Delta^{14}C$ station. Within matched $\Delta^{14}C$ and dCo stations, individual samples were paired if their depth offset was < 100 m. If more than one sample fit this requirement, the closest depth was used.

2.3. Cobalt composition of sinking particles

High-resolution, size fractionated datasets of particulate cobalt are used for two purposes: 1) to document the presence of authigenic cobalt in the mesopelagic zone, and 2) to constrain the downward flux of biogenic cobalt from the surface ocean via the biological pump. The cobalt content of large (> 51 μm) particles were analyzed from samples collected onboard the GA03 (Ohnemus and Lam, 2015) and GP16 transects (Lee et al., In Review). The large size of these particles is thought to represent sinking material in the ocean better than other size classes. Hence, we refer to these as sinking particles. The behavior of Co and P in large particles in both datasets is qualitatively similar to smaller, suspended particles collected by McLane pumps or Go-Flo bottles (at least with respect to Co; Ohnemus and Lam, 2015; Ohnemus et al., 2016; Saito et al., In Review). Sinking particles were collected by McLane pump for both cruises and analyzed as described by Ohnemus and Lam (2015). Filters were initially digested with a sulfuric acid/peroxide mixture, digested fully with 4 N each of HCl, HNO_3, and HF, and subsequently analyzed by ICPMS (Ohnemus and Lam, 2015; Lee et al., In Revision). These datasets are available online as BCO-DMO datasets #3871 and #499723.

Although the pCo:pP ratio from large particles in the upper 100 m varied over two orders of magnitude, both datasets resembled a log-normal distribution (see Fig. 6). The log-transformed Co:P ratio of these samples was binned into histograms of 0.25 log units and fit to a Gaussian function in Sigmaplot 12 to calculate the center (X_0) of each distribution. For the GP16 dataset, 9 samples collected within the OMZ (< 20 μM O_2) were excluded from the calculation of X_0. The value of X_0 was stable over a range of bin sizes (Fig. S3), but at coarser bin resolution X_0 increased and became less constrained, especially in the North Atlantic. The range in X_0 between bin sizes of 0.1–0.5 log units is larger than the standard error in X_0 for any single bin size. As such, the range in X_0 at 0.1 and 0.5 log unit bin sizes is used to estimate the uncertainty from this approach (Fig. S3).

For these analyses, particulate Co and P were corrected for contributions of lithogenic material using Ti measurements and the composition of upper continental crust, as described above (McLennan, 2001). This correction was negligible for P but was important for Co, especially in the GA03 dataset. Notably, aerosol measurements on GA03 support the use of this crustal ratio (Shelley et al., 2015). Due to analytical uncertainty in the measurement of Co and Ti, as well as variability in detrital composition and high dust loadings, lithogenic correction sometimes resulted in a negative concentration of biogenic cobalt (12% of samples for GA03 and 6% for GP16). In order to prevent these negative values from skewing basin scale mean values, these samples were set to a biogenic cobalt concentration of 0. Median biogenic pCo:pP values are unchanged from this correction. By nature, these 0 values cannot be incorporated into analysis of the log-normalized distributions and calculation of X_0. While this procedure has the potential to overestimate pCo:pP stoichiometry by excluding lower values, we note that Ti correction of lithogenic materials has been found to bias towards overcorrection (perhaps due to metal dissolution from dust, Rauschenberg and Twining, 2015), and therefore expect a muted effect.

2.4. Isopycnal scavenging calculations

The cobalt scavenging flux in the mesopelagic (100–1500 m) is calculated as the difference between the sinking flux of biogenic, particulate cobalt below 100 m, and the remineralization of dissolved cobalt within the mesopelagic zone. This approach leverages a consistent offset between high ratios of cobalt and phosphorus in surface ocean particulate matter (pCo:pP) and low mesopelagic ratios of dissolved cobalt and dissolved phosphate (dCo:PO_4), which we interpret as a signature of cobalt scavenging (See Results and discussion for derivation of relevant equations). In the absence of scavenging, the breakdown of biogenic particulate material that sinks below the euphotic zone would be expected to return both nutrients at the same stoichiometry as they are exported from the surface ocean. Cobalt remineralization rates on individual isopycnal surfaces as the product of a dCo:PO_4 stoichiometry and a modeled PO_4 remineralization rate. These were then compared, quantitatively, to the expected stoichiometry based on biogenic pCo:pP ratios from sinking particles collected in the

upper 100 m of both basins, whose degradation rates in the mesopelagic were modeled by the same expression for PO_4 remineralization. Throughout, we distinguish between the *degradation* of biogenic particles (which containing Co and P) and true *remineralization*, defined as the return of cobalt and phosphate to the dissolved phase. The potentially confounding effects of preferential Co or P remineralization are discussed later (see Results and discussion).

Dissolved cobalt (dCo) and phosphate (PO_4) datasets from GP16 in the Eastern Tropical South Pacific and GA03 in the Subtropical North Atlantic were downloaded from the Biological and Chemical Oceanography Data Management Office (BCO-DMO datasets #3868 and #642974; Hawco et al., 2016; Noble et al., 2017). Samples below 1500 m were discarded to avoid double counting with respect to the radiocarbon observations (see above). Datasets were then subdivided by potential density (σ_θ) into 0.25 kg m^{-3} isopycnal bins. This isopycnal bin size was chosen because it enabled the inclusion of > 10 measurements per density strata, even in narrow thermoclines. For GP16, it was necessary to exclude samples collected within the oxygen minimum zone (OMZ, O_2 < 20 μM) due to a clear departure of dCo in these samples compared to the basin scale trend that is driven by a large cobalt source from the Peru Margin (Hawco et al., 2016; Saito et al., 2004). Samples < 10 m were also excluded due to temperature and salinity modification and short-term biological uptake.

The range of included isopycnal surfaces was chosen so that layers reside predominantly in the mesopelagic, between 100 and 1500 m. Shallower isopycnal surfaces were excluded (< 25.375 kg m^{-3} for the GP16 section and < 26.125 kg m^{-3} for the GA03 section), in part because they are mixed on timescales < 5 years, especially in the North Atlantic, and therefore do not represent the same level of integration as the underlying surfaces (Fiedler and Talley, 2006; Jenkins et al., 2015). As a result, shallow dCo:PO_4 relationships are more complex and require fine-scale approaches to derive the stoichiometry of phytoplankton uptake (Saito et al., In Review). Several studies have also shown that manganese and cobalt scavenging in the upper 100 m is very low due to light-driven inhibition and dissolution of bacterial manganese oxides (Moffett and Ho, 1996; Sunda and Huntsman, 1990, 1988), suggesting that excluding these near-surface isopycnals affects scavenging calculations minimally.

Linear regression between dissolved cobalt and phosphate were used to calculate dCo:PO_4 ratios of remineralization on individual isopycnal surfaces. Preformed concentrations of both dCo and PO_4 are reflected in the intercepts of the linear regression rather than their slopes. The value and standard error of the isopycnal dCo:PO_4 slope was calculated by least-squares linear regression with SigmaPlot 12. Mixing of subtropical and tropical water masses with distinct endmember concentrations of dCo and PO_4 will affect the relationship between these two elements. However, most of these water masses on any given isopycnal originate from a similar source region and differ primarily by their age, suggesting that the dominant control of endmember dCo and PO_4 values is the amount of remineralization of both dCo and PO_4 since ventilation, as well as the extent of Co scavenging. Isopycnal mixing will therefore integrate local variability in remineralization and/or scavenging at the basin scale. On individual isopycnal surfaces, there are probably regions where this simplified view is untenable (for instance in the OMZ of the South Pacific (Fig. 5), which has been excluded from these calculations), but the strong covariation between dCo and PO_4 on many of these surfaces implies that the influence of endmember mixing is second to that of remineralization. This approach is not applicable in the deep ocean (> 1500 m) where slow rates of remineralization and scavenging preserve signatures of endmember mixing and dCo and PO_4 are uncorrelated (see Results and discussion, Dulaquais et al., 2014b).

Mesopelagic PO_4-remineralization rates were calculated from region-specific export models of phosphate. The vertical flux of phosphate follows a Martin-curve parameterization:

$$F_z = F_{z*} \times \left(\frac{z}{z^*}\right)^{-b} \quad (2)$$

fit to a global nutrient database via an inverse circulation model (Teng et al., 2014). Parameters used in these calculations are taken from values in Extended Data Figs. 4 and 5 using the flexible C:P stoichiometry scenario from Teng et al. (2014). The critical depth of export, z*, was adjusted from 73.4 m (Teng et al., 2014) to 100 m in order to account for deeper euphotic zones observed on both cruises and to match the isopycnal depth range identified above for dCo:PO_4 correlation. The amount of phosphate exported to a given depth is determined by the phosphate flux at 100 m and the attenuation coefficient, b. As per Teng et al. (2014), both F_{100} and b are unique to biogeochemical province (e.g. subtropical Atlantic, tropical Atlantic).

To counteract sampling bias associated with individual GEOTRACES transects, the mean depth (z_{mean}) of each isopycnal surface was calculated from the WOCE Global Hydrographic Climatology (Gouretski and Koltermann, 2004). The hydrographic domain associated with the zonal GP16 transect was defined by a rectangle spanning the Eastern South Pacific Ocean (5–30°S, 71–150°W); the GA03 transect was defined by a domain between 10 and 45°N and 10–80°W. For consistency with dCo data, depths below 1500 m were removed. The height of each isopycnal box was calculated as the midpoint between z_{mean} of the isopycnal surface and the overlying and underlying boxes.

Optimized multi-parameter water mass analyses have indicated that mesopelagic waters sampled on the GA03 and GP16 transects contain mixtures of subtropical and tropical water masses (Jenkins et al., 2014; Peters et al., In Review). To account for the presence of remineralized nutrients exported from both subtropical and tropical provinces, P-remineralization equations were modified so that 'b' and F_{100} express the weighted average of Eq. (2), based on the phosphate export at 100 m from both provinces (Table 3). Over 90% of the P-flux is remineralized between 100 and 1500 m, the size of the mesopelagic box used here. This is consistent with very low remineralization rates in the deep ocean inferred by correlations between radiocarbon age and apparent oxygen utilization (Broecker et al., 1991; Karstensen et al., 2008).

Isopycnal P remineralization rates (in mol m^{-2} $year^{-1}$) are

Table 3
Phosphate export parameters derived from Teng et al., 2014. Fluxes are modified to reflect export at 100 m. Averages of Tropical and Subtropical domains, weighted by total P export, are used to calculate dCo:$PO_{4,remin}$.

	P export Tmol $year^{-1}$[a]	P export, 100 m mmol m^{-2} $year^{-1}$	P-attenuation 'b' exponent[a]	Export weighted dCo:$PO_{4,remin}$, μmol:mol
North Atlantic (GA03)				
Subtropical	0.21	7.7	1.3	60.8 ± 6.5
Tropical	0.29	17.8	0.76	56.0 ± 4.9
Weighted average		13.5	0.99	58.4 ± 5.6
South Pacific (GP16)				
Subtropical	0.35	10.9	1.33	82.3 ± 7.1
Tropical	0.90	17.9	0.71	69.1 ± 5.3
Weighted average		15.9	0.88	73.1 ± 5.8

[a] As published in Teng et al. (2014).

calculated as the difference between the P flux at the upper bound and lower bound of a given isopycnal box. A 20% uncertainty in P remineralization rates is applied, which represents the upper end of uncertainty suggested by Teng et al. (2014). These values were used to weight isopycnal $dCo:PO_4$ slope to derive a $dCo:PO_4$ stoichiometry of remineralization ($dCo:PO_{4,\ remin}$). $dCo:PO_{4,\ remin}$ is independent of the actual magnitude of the P flux but depends on the attenuation of 'b'. This dependence was evaluated for a range of 'b' relevant to the ocean (Fig. S4; Teng et al., 2014). $dCo:PO_{4,\ remin}$ increases somewhat with increasing 'b' but the effect is small, at least in comparison to the magnitude of the pCo:pP ratio in sinking particles.

The major sources of uncertainty in calculating scavenging fluxes with this approach are 1) the 20% uncertainty in P-remineralization rates, 2) uncertainties in the slope of the isopycnal $dCo:PO_4$ relationship, determined by standard error of the slope of linear regression and 3) the estimation of the basin average pCo:pP ratio of exported biomass.

3. Results and discussion

3.1. The Marine Co sink

The degree of cobalt enrichment in marine sediments is inversely related to the rate of sediment accumulation: the highest cobalt content characterizes the slowest accumulating sediments (Fig. 1; Krishnaswami, 1976). These observations have been explained by considering sedimentary Co content as a mixture of a major, Co-poor component from dust and continental detritus with a minor, Co-rich component from the water column, such as Mn-oxides (Goldberg and Arrhenius, 1958; Krishnaswami, 1976). Because oxygen is abundant in pelagic sediment porewaters and Co contents of other common sedimentary phases are low, complication of this simple model by hydrothermalism, biomineral deposition, or reductive remobilization of authigenic Co is minimal (D'Hondt et al., 2015; Dunlea et al., 2015; Kyte et al., 1993). This sedimentary perspective is consistent with water column measurements showing very small hydrothermal and benthic inputs of Co to the deep ocean (Hawco et al., 2016; Noble et al., 2012). Therefore, when the mass accumulation rate of sediments is known, the flux of the authigenic component (K, in μmol m^{-2} $year^{-1}$) can be calculated as:

$$K = S_m \times (Co_{sediment} - Co_{detrital}) \quad (3)$$

where $Co_{detrital}$ reflects the Co content in upper continental crust (17 ppm, or by correction with Ti, McLennan, 2001) and S_m is the mass

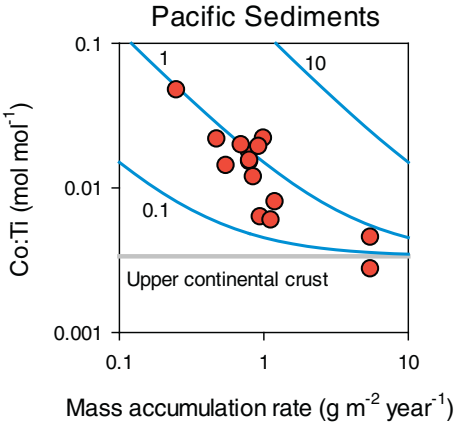

Fig. 1. The Co:Ti ratio in Quaternary Pacific Ocean sediments. Co:Ti increases with decreasing mass accumulation rate. At high accumulation rates, Co:Ti matches Upper Continental Crust (3.37×10^{-3} M M^{-1}, McLennan, 2001). Blue lines show calculated rates of the authigenic Co flux, K, in μmol m^{-2} $year^{-1}$. (For interpretation of the references to colour in this figure legend, the reader is referred to the web version of this article.)
Replotted from Krishnaswami (1976).

accumulation rate for bulk sediments in g m^{-2} $year^{-1}$. Early investigations noted the apparent similarity in K both downcore and across spatial gradients in surface sediments, resulting in the assertion that the rate of authigenic Co accumulation, K, is nearly constant on timescales of 10^5 years and longer (Kadko, 1985; Krishnaswami, 1976).

Yet, there is an 8-fold variation in published rates of K (Table 1), ranging from 0.34 μmol m^{-2} $year^{-1}$ from the South Pacific gyre to 2.3 μmol m^{-2} $year^{-1}$ in the Sargasso Sea. Thus, as discussed previously, authigenic Co accumulation rates in sediments are not strictly constant (Dunlea et al., 2015). Determinations of K in Quaternary sediments tend to be higher in the Atlantic than the Pacific. Furthermore, in the Pacific Ocean, Quaternary sediments in Table 1 indicate higher rates of K than records that span the entire Cenozoic era (65 Mya). This suggestion echoes downcore observations from Kyte et al. (1993), who used stratigraphic constraints to show an increase in authigenic Co accumulation in the North Pacific since the onset of the Pliocene (2.5–5 Mya). It appears significant that Cenozoic estimates of K (0.34–0.44 μmol m^{-2} $year^{-1}$) converge with accumulation rates in Mn nodules and ferromanganese crusts (0.32–0.40 μmol m^{-2} $year^{-1}$), as both integrate over similar 10^6–10^7 year timescales (Dunlea et al., 2015; Frank et al., 1999; Halbach et al., 1983; Kyte et al., 1993; Zhou and Kyte, 1992). This similarity suggests that sediments, nodules, and ferromanganese crusts accumulate cobalt from a similar water column source and support the assertion that cobalt accumulation rates were lower before the Pleistocene (Kyte et al., 1993). We are unaware of records that span a similar timescale in the Atlantic, Indian or Southern Oceans to confirm or negate this hypothesis.

While the cause of the differences in K is unknown, general agreement in Quaternary sediments between multiple investigations enables a reasonable estimation of the pelagic cobalt sink for each basin. Average authigenic cobalt accumulation rates in Quaternary sediments in the Atlantic and Pacific (1.9 and 1.1 μmol m^{-2} $year^{-1}$, respectively) imply a global sink on the order of 450 Mmol Co $year^{-1}$ (see Methods for details). Against an average oceanic concentration of 46 pM, estimated from recent GEOTRACES data (Fig. S1), this sink corresponds to a total ocean residence time of 130 years. As the ~10^5 year time-scale of authigenic Co determination in sediments integrates over dozens of revolutions of the oceanic cobalt cycle, stabilizing mechanisms on either water column scavenging processes or cobalt sources must be substantial if the flux to marine sediments (K) is actually steady. To shed light on these controls, water column scavenging processes are investigated in the following sections using a wealth of new dissolved and particulate cobalt measurements from GEOTRACES datasets in the Atlantic and Pacific basins.

3.2. Deep ocean scavenging

Scaling cobalt accumulation rates in pelagic sediments to an average ocean depth of 3700 m suggests a mean scavenging rate of 0.3–0.5 pM per year. But is this process uniform in the water column? Below 1000 m, profiles from the Atlantic and Pacific show that dCo decreases along the path of the meridional overturning circulation (Fig. 2a, Fig. S1). dCo concentrations decrease from 50 to 100 pM in the deep North Atlantic from 20 to 40 pM in Antarctic and Pacific deep waters.

To trace the loss of dCo from deep waters during the meridional overturning circulation, recently collected dCo datasets were compared with the radiocarbon content of dissolved inorganic carbon ($\Delta^{14}C$), which enters the deep ocean almost exclusively via formation of North Atlantic Deep Water (NADW; Broecker et al., 1991). Regional averages of dCo for each of these transects across bathypelagic (1500–3000 m) and bottom waters (> 3000 m) were compared to $\Delta^{14}C$ measurements from the GLODAP database over a similar spatial domain (Key et al., 2004). dCo in the deep ocean follows a linear relationship with $\Delta^{14}C$. As $\Delta^{14}C$ describes both the mixing of NADW and the aging of those mixtures in the overturning circulation (Broecker et al., 1991; Matsumoto, 2007), the correlation with dCo implies that cobalt scavenging in the

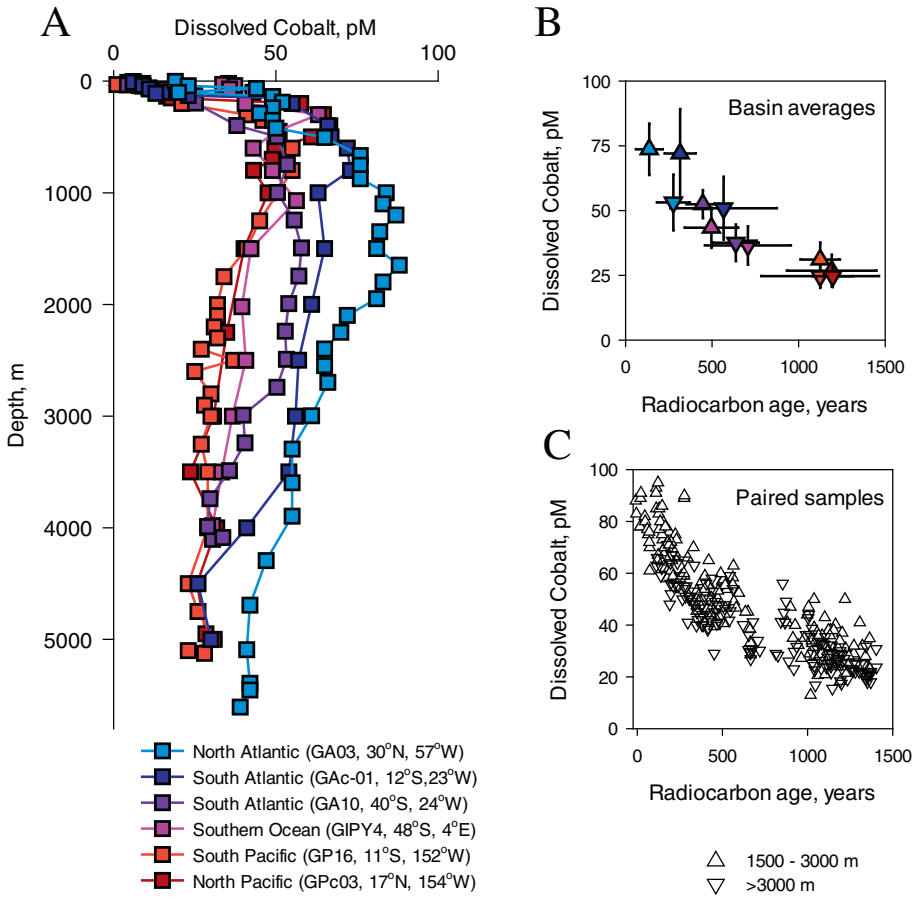

Fig. 2. Removal of dissolved cobalt from the deep ocean. A) Dissolved cobalt profiles collected from several ocean basins. B) Mean dissolved cobalt concentrations from GEOTRACES sections with the natural radiocarbon age averaged over a similar spatial scale in the GLODAP database (Table 2). Colors of datasets correspond to those in A; upward pointing triangles describe samples collected between 1500 and 3000 m while downward pointing triangles describe samples collected deeper than 3000 m. B) Individually paired dissolved cobalt measurements from GEOTRACES transects with co-located measurements of the natural radiocarbon age from GLODAP (see Methods).

deep ocean occurs on a similar timescale to ^{14}C decay.

Converting to radiocarbon age by solving the half-life equation for ^{14}C produces an exponential relationship with dCo (Fig. 2b). Fit to Fig. 2b, deep ocean dCo follows the equation:

$$dCo = 83 \times e^{-1.02\times10^{-3}\times\tau} \quad (4)$$

where τ is the natural $\Delta^{14}C$ age in years ($r^2 = 0.88$). From this regression, the net rate of scavenging over 1500 years is calculated as 0.043 pM $year^{-1}$ and, from the reciprocal of the coefficient in the exponent (1.02×10^{-3} $year^{-1}$), a residence time can be inferred. Dissolved cobalt in the deep ocean (> 1500 m) has a turnover time of 980 years, nearly an order of magnitude longer than the whole ocean residence time calculated by cobalt accumulation rates in pelagic sediments!

Pairing over 300 dCo measurements with co-located $\Delta^{14}C$ measurements from GLODAP shows that the exponential relationship between dCo and age holds on a sample-by-sample basis (Fig. 2c), implying slow and steady removal of cobalt as the deep ocean ages. Because the dCo concentration of southern-sourced waters is considerably less than the deep North Atlantic, deep water formation in the Southern Ocean adds little dCo to deep waters. Unlike nanomolar dCo that is typical of temperate estuaries in North America, dCo in the Ross and Weddell Seas is typically < 100 pM, indicating only a small Co source from glacial weathering on the Antarctic continent (Bown et al., 2011; Saito et al., 2010; Sañudo-Wilhelmy et al., 2002; Tovar-Sánchez et al., 2004). Due to slow timescales of ^{14}C equilibration with the atmosphere, Antarctic deep water formation also lacks a distinct $\Delta^{14}C$ signature. As a result, the relationship between dCo and $\Delta^{14}C$ age is not improved by accounting for deep water formation in the Southern Ocean (e.g. Matsumoto, 2007; Fig. S2). Like $\Delta^{14}C$, most dCo in deep waters derives from NADW.

This analysis expands on observations from a meridional transect in the Western Atlantic, which attributed decreasing dCo on isopycnal surfaces to mixing between NADW and Antarctic Bottom Water (AABW) water types (Dulaquais et al., 2014b). This was followed by the suggestion that dCo scavenging was negligible in Atlantic deep waters (Dulaquais et al., 2014b). While a shared source in NADW can generate a correlation between $\Delta^{14}C$ and dCo by mixing, there must be some removal of cobalt in the deep ocean by scavenging in order to keep pace with the loss of $\Delta^{14}C$ due to radioactive decay. As the meridional transit time of NADW in the deep Atlantic is on the order of 200 years (Broecker et al., 1991; Matsumoto, 2007) – about a quarter of the cobalt scavenging turnover time from Eq. (4) – it may be difficult to distinguish scavenging from water mass mixing in the deep Atlantic Ocean.

While this correlation constrains the timescale of cobalt scavenging, the underlying mechanism remains enigmatic. It is unlikely that cobalt scavenging in the deep ocean is restricted to specific environments such as hydrothermal plumes or continental slopes, as both have been sampled by the GEOTRACES program and do not show evidence for quantitative dCo removal (Dulaquais et al., 2014b; Hawco et al., 2016; Noble et al., 2017). Abiotic rates of inorganic manganese oxidation in seawater are dependent on the concentrations of manganese (II) ion, hydroxide ion, and dissolved oxygen (von Langen et al., 1997), but bacterial enzymes can also catalyze this reaction (Moffett and Ho, 1996). As the redox chemistry of cobalt and manganese are similar, abiotic or biotic manganese oxidation may remove kinetically labile cobalt species via co-oxidation. For cobalt bound to strong organic ligands, however, additional photochemical or biological processing may be required before it can be scavenged by this mechanism; there may be other pathways of cobalt removal in the deep sea.

Scaling the apparent rate of dCo removal in the deep ocean from Eq. (4) (0.043 pM $year^{-1}$) to the depth of the deep ocean (1500–3700 m)

suggests an areal flux of 0.09 μmol m^{-2} $year^{-1}$, far less than the 0.9–2.5 μmol m^{-2} $year^{-1}$ expected from cobalt accumulation rates in Quaternary sediments (Table 1). More than half the volume of the ocean provides only ~10% of the Co delivered to marine sediments. Either these sediment fluxes are severely overestimated or the remainder of the scavenged Co flux to marine sediments must be balanced by scavenging in the upper ocean.

3.3. Authigenic cobalt formation in the mesopelagic

In the upper ocean (< 1500 m), Co is strongly influenced by nutrient uptake and regeneration, which mask signatures of water-column scavenging in the dissolved Co profile (Fig. 2a; Dulaquais et al., 2014b; Noble et al., 2012; Saito and Moffett, 2002). In order to appreciate how scavenging affects the Co inventory here, the biological Co cycle must first be understood and quantified. Yet, phytoplankton Co quotas are not uniform across species and are influenced by both the availability of other nutrients (e.g. Zn, P) and by the complexation of dCo in the surface ocean, making the amount of remineralized Co in any given water parcel difficult to predict a priori (Jakuba et al., 2008; Saito and Moffett, 2001; Shaked et al., 2006; Sunda and Huntsman, 1995).

Examining particulate Co distributions can provide important constraints on cobalt scavenging in the upper ocean. Datasets from GEOTRACES sections in the North Atlantic (GA03) and South Pacific (GP16) indicate that cobalt in large (> 51 μm), sinking particles represents a combination of lithogenic, biogenic, and authigenic phases (Fig. 3). Using particulate Ti (pTi) as a tracer of lithogenic material, particles containing a Co:Ti ratio near the continental crust ratio (3.37×10^{-3} mol mol^{-1}) are expected to reflect a large contribution of dust or continental sediments to the pCo inventory (McLennan, 2001; Ohnemus and Lam, 2015). This crustal Co:Ti ratio is almost identical to the slope of aerosol Co and Ti in the North Atlantic, 3.40×10^{-3} mol mol^{-1} (R^2 = 0.995, Shelley et al., 2015). Even in the dust-heavy North Atlantic, however, pCo:pTi is in excess of continental crust (i.e. dust) throughout the upper water column, especially in the upper 300 m, signifying the predominance of biogenic and authigenic (i.e. scavenged) components in these basins (Fig. 3a, S5).

Biogenic Co, in turn, can be traced by particulate phosphorus (pP). Biological uptake of PO_4 by phytoplankton results in a near-surface maximum of pP that decreases sharply with depth (Ohnemus and Lam, 2015). Although nutrient cycling of Co results in pCo profiles that share these features, this gradient is stunted in comparison to pP, leading to pCo:pP ratios that increase with depth (Fig. 3b). Thus, the pCo concentration in sinking particles in the mesopelagic zone of the North Atlantic and South Pacific is too high to be accurately reflected by biogenic or lithogenic phases, signifying a major contribution from an authigenic (i.e. scavenged) phase at these depths. When normalized to pTi or pP, particulate concentrations of Co and Mn between 100 and 1500 m are extremely well correlated (Fig. 3c, d), strongly suggesting Mn-oxide phases make up the bulk of the particulate cobalt sinking below the mesopelagic in both basins, similar to observations of Co and Mn in smaller, suspended particles (Lee et al., In Review; Saito et al., In Review). Aggregation of authigenic cobalt in smaller particles with lithogenic and biogenic particles may contribute to their downward export to the sediments (Ohnemus and Lam, 2015).

3.4. A remineralization – scavenging framework

Here, we describe an empirical approach to calculate cobalt scavenging rates in the upper ocean. Dissolved phase dCo:PO_4 ratios in

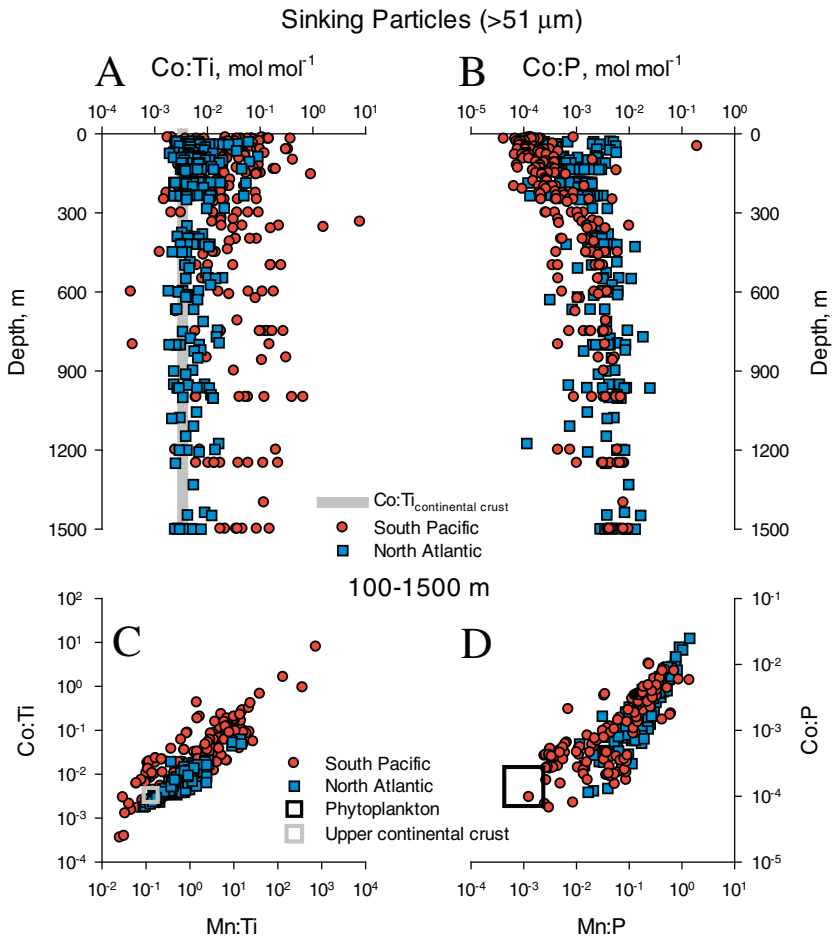

Fig. 3. Cobalt in large (> 51 μm) particles in the North Atlantic and South Pacific. A) The pCo:pTi ratio in large sinking particles from the North Atlantic (blue squares) and South Pacific (red circles) transects. The grey line shows the Co:Ti ratio of upper continental crust (3.37×10^{-3} mol mol^{-1} from McLennan, 2001). B) The pCo:pP ratios in the same datasets. C) Correlations between Ti-normalized Co and Mn in the mesopelagic. Crustal ratios from McLennan (2001) are plotted as a grey square. D) P-normalized Co and Mn. The abundance of both metals in phytoplankton biomass, estimated from Twining and Baines (2013), is plotted as a black square in panel D. Because particulate Co and Mn in the mesopelagic (100–1500 m) are in excess of phytoplankton and crustal sources, cobalt is probably in a manganese oxide phase. Note that the size of the squares in C and D are chosen for clarity and do not necessarily reflect variability associated with these values. (For interpretation of the references to colour in this figure legend, the reader is referred to the web version of this article.)

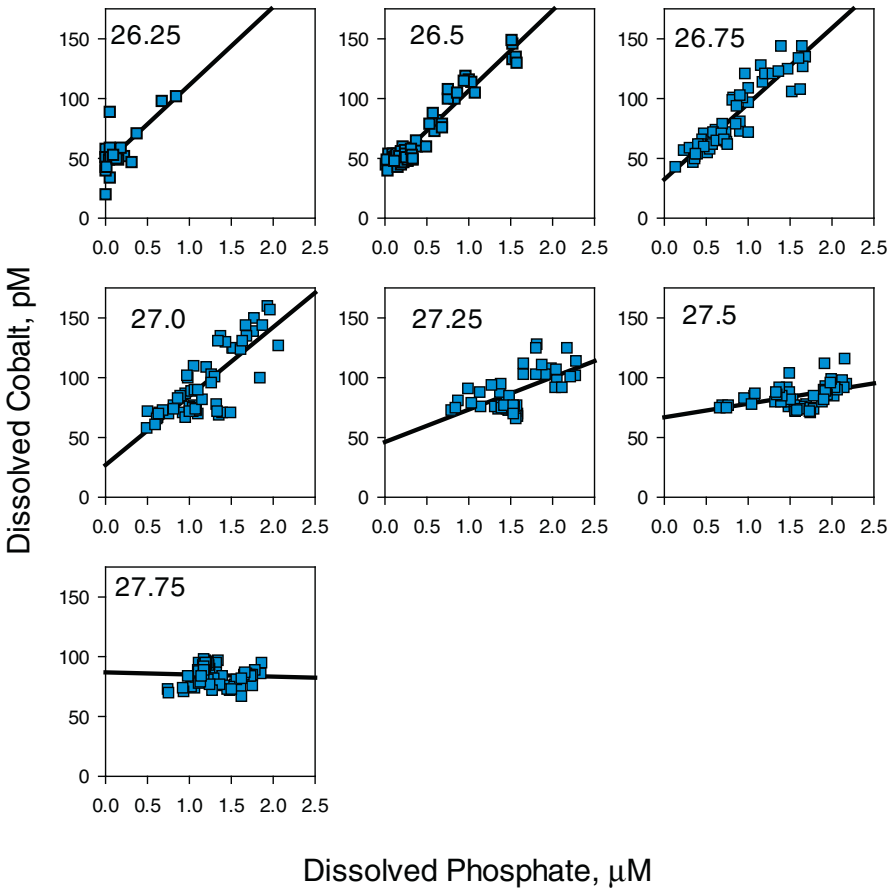

Fig. 4. Isopycnal relationships between dissolved cobalt and phosphate in the North Atlantic Ocean (GA03). Best fit lines are shown as 1σ range of the regression (slope and intercept). See Table 4.

the mesopelagic are lower than both particulate pCo:P at the same depth and from those sampled in the euphotic zone. Assuming that most of the sinking flux of pP from the euphotic zone is remineralized to dissolved PO_4 in the mesopelagic (< 1500 m), the low dCo:PO_4 ratios reflect an incomplete return of biogenic pCo to the dissolved phase during remineralization due to cobalt scavenging onto manganese oxides.

As mixing in the oceans occurs predominantly between waters of similar density, integration over isopycnal surfaces can be used to trace dCo and PO_4 remineralization on the basin scale. Narrow isopycnal surfaces (± 0.125 kg m^{-3}) are well-sampled in the GA03 and GP16 datasets in the North Atlantic and South Pacific (> 10 discrete measurements per density interval) and show strong coupling between dCo and PO_4 along almost all isopycnal windows in the mesopelagic zone (100–1500 m). Because these waters are constantly receiving a flux of organic matter from overlying waters (containing both pCo and pP), positive correlations between these two parameters in both the North Atlantic (Fig. 4) and South Pacific Oceans (Fig. 5) confirm that remineralization is a major process affecting dCo distributions.

A major exception to these basin scale trends can be seen in the oxygen minimum zone (OMZ) of the South Pacific (Fig. 5). At O_2 < 20 µM, dCo shows sharp, PO_4-independent increases that reflect redox-related Co cycling associated with a source from reducing shelf sediments (Hawco et al., 2016). As a result, we have excluded samples collected in the OMZ (O_2 < 20 µM) when interpreting isopycnal dCo:PO_4 slopes (see Methods). Oxic samples on these isopycnal layers, however, follow low dCo:PO_4 slopes (Fig. 5, red circles), implying that lateral ventilation of OMZ waters by oxygenated, subtropical water masses removes the excess dCo that had accumulated in the OMZ while reducing conditions prevailed.

Because of widespread correlations between dCo and PO_4 on isopycnal surfaces and the absence of meaningful PO_4 scavenging, we can use PO_4 remineralization to trace dCo remineralization in the water column. On any isopycnal surface, the rate of dCo remineralization from sinking biomass: $J_{remin.}$(dCo), can be approximated as the rate of PO_4 remineralization and the slope of the dCo:PO_4 relationship:

$$J_{remin.}(dCo) = dCo{:}\ PO_{4isopycnal} \times J_{remin.}(PO_4) \quad (5)$$

where the rate of PO_4 remineralization, $J_{remin.}(PO_4)$, is calculated from a depth-dependent power function fit to global phosphate distributions (Teng et al., 2014). By weighting each isopycnal dCo:PO_4 slope by the amount of PO_4 remineralization within that isopycnal window, an areal remineralization stoichiometry, $dCo{:}PO_{4,remin}$, can be derived (Table 4). In the North Atlantic, remineralization of 12.6 mmol m^{-2} $year^{-1}$ of PO_4 between 100 and 1500 m coincides with the remineralization of 735 ± 110 nmol m^{-2} $year^{-1}$ of dCo, resulting in a value of $dCo{:}PO_{4,remin}$ in the North Atlantic of 58.4 ± 5.6 µmol:mol, slightly lower than that derived for the South Pacific, 73.1 ± 5.8 µmol:mol (Table 4, S1). This difference is largely due to the offset between dCo:PO_4 ratios in the shallowest isopycnal surfaces.

Since large particles are subject to strong settling forces, the particulate Co and P datasets for large (> 51 µm) particles from the upper 100 m of the North Atlantic and South Pacific GEOTRACES transects (GA03 and GP16) can be compared to the $dCo{:}PO_{4,remin}$ ratios determined above. In order to estimate biogenic cobalt, the high contribution of dust in the North Atlantic first requires a subtraction of lithogenic Co, calculated from the pTi concentration and the molar Co:Ti ratio in upper continental crust, 3.37×10^{-3}. In the Atlantic, pCo:pP values in samples corrected for detrital Co are significantly lower than uncorrected (Fig. 6a), while in the South Pacific, detrital correction affects the pCo:pP ratio minimally (Fig. 6b). Despite 100-fold variability in Ti-corrected pCo:pP, most of the measurements in both basins have biogenic pCo:pP ratios > 100 µmol mol^{-1}, higher than

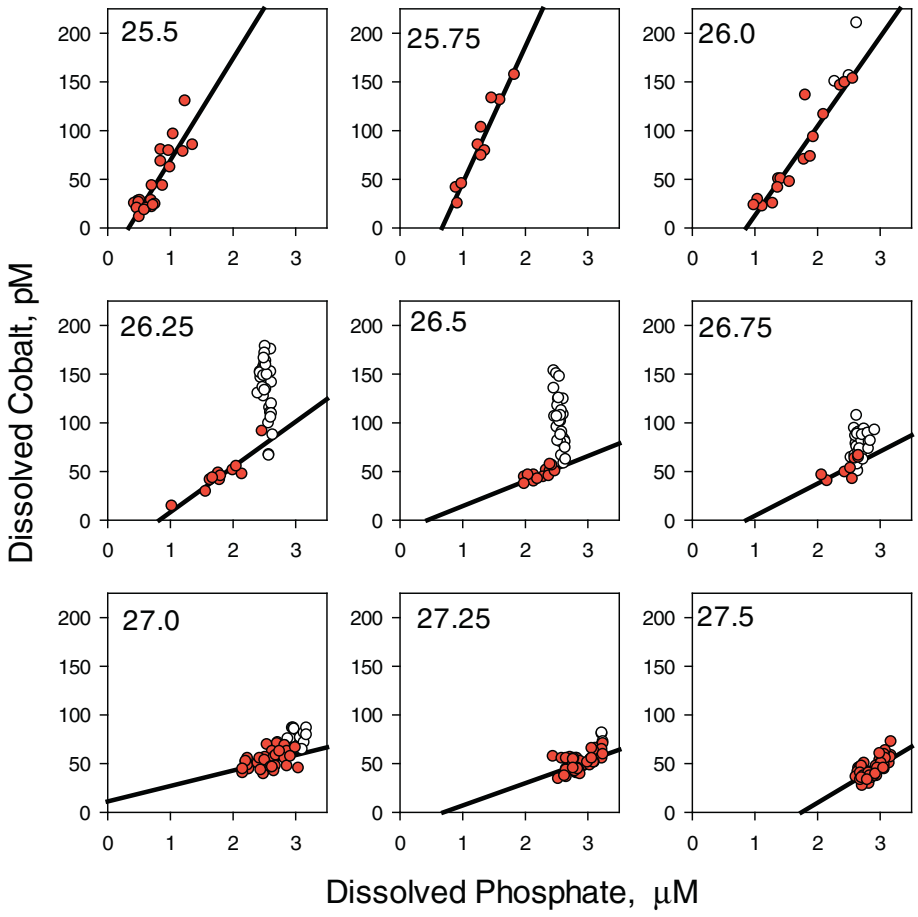

Fig. 5. Isopycnal relationships between dissolved cobalt and phosphate in the South Pacific Ocean (GP16). Low oxygen samples (O_2 < 20 µM, white circles) are highlighted and excluded from calculation of dCo:PO_4 slopes due to the influence of a large cobalt source from the Peru shelf. Best fit lines are shown as 1σ range of the regression (slope and intercept). See Table 4.

the dCo:$PO_{4,remin}$ ratios calculated above. In fact only 20% of large particles in the upper 100 m of both basins have a biogenic pCo:pP ratio less than or equal to these remineralization stoichiometries. Thus, cobalt does not seem to be conserved during remineralization: there is more cobalt exported from the surface ocean in biogenic particles than reappears as dissolved cobalt in the mesopelagic.

Differences between upper ocean cycles of cobalt and phosphate can be exploited to estimate rates of mesopelagic cobalt scavenging. Here, it is useful to differentiate between two related processes: 1) pCo degradation and 2) dCo remineralization. pCo degradation, $J_{degrad.}(pCo)$, is the disintegration of cobalt-bearing biogenic phases through heterotrophic respiration on sinking particles. dCo remineralization, instead, represents the explicit (and measurable) return of cobalt to the dissolved phase of seawater. The difference between the two is the scavenging flux of cobalt, $J_{scavenging}(Co)$:

$$J_{scavenging}(Co) = J_{degrad.}(pCo) - J_{remin.}(dCo) \quad (6)$$

where the units for the above terms are mol m^{-3} $year^{-1}$. For typical nutrients such as P, particulate degradation and dissolved remineralization processes are identical; yet for elements with a propensity to scavenge, a 'degradation' flux may be larger than the observed remineralization of dissolved species, as suggested by higher pCo:pP in particles sinking from the euphotic zone than the dCo:$PO_{4,remin}$ determined in the mesopelagic.

The rate that sinking biogenic Co is degraded, can be calculated as the product of the P remineralization rate and the pCo:pP composition of sinking organic matter:

$$J_{degrad.}(pCo) = \left(\frac{pCo}{pP}\right)_{export} \times J_{remin.}(PO_4) \quad (7)$$

Thus, Eq. (7) provides an expected return of Co to the water column during remineralization, whereas Eq. (5) describes the actual return. Diverse micronutrient use of cobalt contributes to variable phytoplankton pCo:pP in the euphotic zone (Sunda and Huntsman, 1995; Saito et al., In Review), making it difficult to estimate a single value of $pCo:pP_{export}$. Despite this variability, histograms of the biogenic pCo:pP ratio in large particles approximate a log-normal distribution, whose center (X_0) can be interpreted as the most probable ratio of Co and P that would be supplied to the mesopelagic via the biological pump (Fig. 6, Table 5). For the North Atlantic, this value was 166 µmol:mol and 116 µmol:mol in the South Pacific, similar to median pCo:pP values for these datasets (Table 5) and within the range of Co quotas observed by phytoplankton in culture (Sunda and Huntsman, 1995; Xu et al., 2007).

In the South Pacific, calculated pCo degradation and dCo remineralization rates are nearly equal in the shallow isopycnals, but decouple near σ_θ = 26.25 (~230 m), where dCo remineralization rates are significantly less than pCo degradation rates (Fig. 7a, Table 4, S2). In contrast, the North Atlantic shows consistent offsets between degradation and remineralization throughout the mesopelagic (Fig. 7c). In the euphotic zone of the North Atlantic, however, dissolved dCo:PO_4 ratios in the North Atlantic do approach those in particles, but congruency between dissolved and particulate ratios is restricted to extremely shallow waters where, in addition to greater biological demand, sunlight inhibits cobalt and manganese scavenging (Sunda and Huntsman, 1988; Saito et al., In Review).

In both basins, rates of expected pCo degradation are greater than apparent remineralization of dCo. If the difference in these processes is attributed to Co removal via scavenging, the rate of Co scavenging on an isopycnal surface can be estimated by substituting Eqs. (5) and (7) into Eq. (6):

Table 4
Mesopelagic cobalt scavenging calculations, calculated based on the difference between particulate Co degradation rates and dissolved Co remineralization rates. Remineralization rates are calculated as the product of P remineralization and the dCo:P ratio on isopycnal surfaces (see Figs. 5 and 6). Degradation rates are calculated as the product of P remineralization and the Co:P ratio of exported biomass ($Co:P_{export}$, see Fig. 7). z_{upper} represents the upper bound of the isopycnal window, calculated as the sum of the mean isopycnal depth (z_{mean}) and half of the height of the isopycnal window (dz).

South Pacific (GP16)						mmol m^{-2} $year^{-1}$	μmol m^{-2} $year^{-1}$		
σ_θ	z_{upper}	dz	dCo:P	±	R^2	$J_{remin.}(PO_4)$	$J_{degrad.}(pCo)$[a]	$J_{remin.}(dCo)$	$J_{scavenging}$ (Co)
25.5	100	67	104.4	13.3	0.75	5.8	0.68	0.61	0.07
25.75	167	28	139.9	14.7	0.92	1.3	0.15	0.18	−0.03
26	195	27	91.6	8.7	0.89	0.9	0.11	0.09	0.02
26.25	222	27	46.5	6.4	0.84	0.8	0.09	0.04	0.05
26.5	249	75	25.7	6.2	0.57	1.5	0.17	0.04	0.13
26.75	325	126	33.1	12.9	0.52	1.4	0.16	0.05	0.12
27	451	246	15.9	5.4	0.19	1.3	0.16	0.02	0.13
27.25	697	322	22.9	5.1	0.32	0.8	0.09	0.02	0.08
27.5	1020	480	38.3	4.7	0.51	0.6	0.07	0.02	0.05
	1500					1.5	0.17	0.11	0.06[b]
P weighted average			73.1	100–1500 m sum		14.4	1.68	1.06	0.62
1σ range			5.8	1σ range		11.5–17.3	1.52–1.86	0.90–1.21	0.40–0.86
				Total		15.9	1.84	1.16	0.68
				1σ range		12.7–19.1	1.47–2.29	0.91–1.41	0.50–0.98
North Atlantic (GA03)									
26.25	100	64	65.3	12.9	0.56	5.4	0.89	0.35	0.54
26.5	167	86	67.1	2.0	0.94	3.1	0.52	0.21	0.31
26.75	272	104	63.2	3.7	0.85	1.2	0.20	0.08	0.12
27	359	186	57.6	5.7	0.65	1.2	0.20	0.07	0.13
27.25	530	253	27.1	5.4	0.37	0.9	0.15	0.02	0.12
27.5	806	313	11.4	3.0	0.21	0.5	0.08	0.01	0.07
27.75	1100	278	−1.8	3.7	0.00	0.3	0.06	0.00	0.06
	1500					0.9	0.15	0.05	0.10[b]
P weighted average			58.4	100–1500 m sum		12.6	2.10	0.74	1.36
1σ range			5.6	1σ range		10.1–15.1	1.86–2.45	0.63–0.85	1.10–1.73
				Total sum		13.5	2.25	0.79	1.46
				1σ range		10.8–16.2	1.76–2.99	0.61–0.93	1.10–2.11

[a] Calculated using a $pCo:pP_{export}$ stoichiometry of 116 for the South Pacific and 166 for the North Atlantic, see Table 5.
[b] Calculated using the aggregate ratio of $J_{remin.}(dCo)$ and $J_{remin.}(PO_4)$ between 100 and 1500 m, i.e. $dCo:PO_{4,remin.}$

$$J_{scavenging}(Co) = J_{remin.}(PO_4) \times \left(\left(\frac{pCo}{pP} \right)_{export} - \left(\frac{dCo}{PO_4} \right)_{isopyncal} \right) \quad (8)$$

Defined as such, the North Atlantic and South Pacific show distinct profiles of scavenging rates (Fig. 7b, d). In the North Atlantic, scavenging appears fastest at ~150 m and decreases with depth (Fig. 7d). This is consistent with ^{55}Mn radiotracer experiments in the Sargasso Sea (Sunda and Huntsman, 1988), which show that rates of heterotrophic Mn oxidation are highest just below the chlorophyll maximum where supply of labile organic matter is high but light levels are low enough to limit photo-reduction and dissolution of particulate Mn-oxides.

In contrast, the profile of the Co scavenging rate in the South Pacific shows low values in shallow waters (z_{mean} < 200 m), and peak scavenging rates at ~300 m (Fig. 7b). Faster rates of PO_4 remineralization and a smaller difference between $pCo:pP_{export}$ and isopycnal $dCo:PO_4$ on these shallow density strata make the scavenging profile in the upper 300 m subject to large uncertainties. However, these results are corroborated by particulate metal inventories measured on this transect, which show that authigenic cobalt in the South Pacific peaks between 200 and 600 m (Lee et al., In Review), similar to the distribution suggested by our calculations. Interestingly, the onset of authigenic cobalt in the South Pacific is deeper than the onset of authigenic Mn, and is consistent with the absence of labile dissolved cobalt in upper 300 m (Hawco et al., 2016; Ohnemus et al., 2016; Lee et al., In Review). It is likely that low concentrations of labile dissolved cobalt in

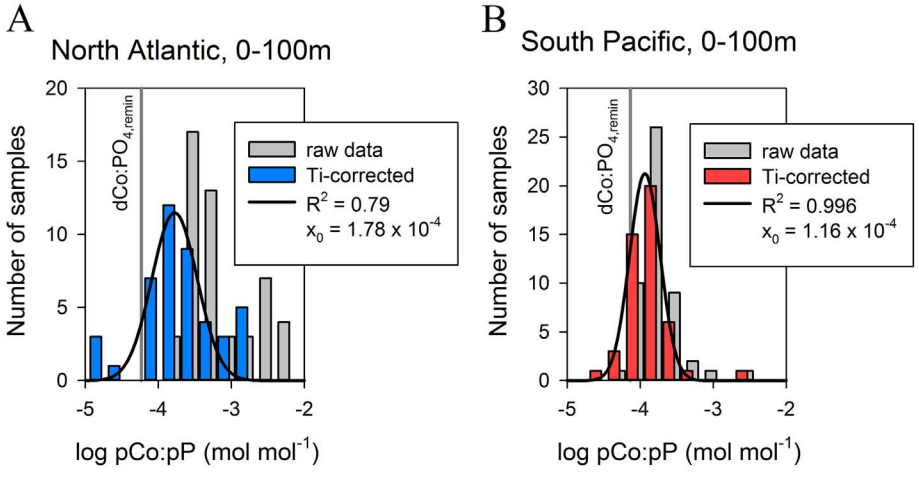

Fig. 6. The stoichiometry of biogenic cobalt and phosphorus in the North Atlantic and South Pacific. Histograms of pCo:pP ratios in large particles for the North Atlantic (A) and South Pacific (B) show log-normal distributions. Lithogenic cobalt was subtracted using particulate Ti concentrations and the Co:Ti ratio of continental crust (3.37×10^{-3} mol mol^{-1}, McLennan, 2001). A small number of samples showed negative values after this correction, and could not be included. Gaussian curves were fit to the Ti-corrected values with the center (X_0) of each curve used to constrain the average pCo:pP stoichiometry of biological export for each basin. Vertical grey lines show export weighted values of $dCo:PO_{4,remin}$ based on dissolved cobalt and phosphate measurements in the mesopelagic (100–1500 m), calculated from Table 4.

Table 5
Comparison of statistics for calculating $pCo:pP_{export}$ from measurements of large (> 51 μm) particles in the upper ocean (0–100 m). All values are in μmol:mol. Ti-correction for detrital cobalt was conducted with a Co:Ti ratio of 3.37×10^{-3} mol:mol. Histograms center values are determined using a bin size of 0.25 log units (Fig. 7). Scavenging calculations employ the Ti-corrected histogram center values, in bold.

	Uncorrected	Ti-corrected
Eastern Tropical South Pacific		
Range	42–2065	0–2051[a]
Mean	196	157 (136)[b]
Median	128	108
Histogram center, X_0	137	**116**
X_0 uncertainty		**111–132**
Dissolved $Co:P_{remin}$[c]		73.1 ± 5.8
Subtropical North Atlantic		
Range	105–5560	0–1552[a]
Mean	1036	301 (126)[b]
Median	355	145
Histogram center, X_0	308	**166**
X_0 uncertainty		**152–209**
Dissolved $Co:P_{remin}$[c]		58.4 ± 5.6

Ti-correction. Both datasets have 50 samples total.
[a] 3 South Pacific and 6 North Atlantic samples have negative values after.
[b] First set of values is calculated if negative values of biogenic cobalt are set to 0. Values in parentheses are calculated with negative values intact.
[c] Weighted average of slopes of isopycnal dCo and PO_4 relationships (Table 2).

the South Pacific limit cobalt scavenging on shallow isopycnal surfaces where dissolved Mn is abundant.

Below 300 m, scavenging rates in both basins taper off. A caveat to the scavenging profiles shown in Fig. 7 is that this shape will change if dCo or PO_4 is preferentially remineralized. Preferential release of PO_4 relative to dCo would cause $pCo:pP_{export}$ to increase with depth, resulting in a more uniform profile of the cobalt scavenging rate. Preferential dCo remineralization, in contrast, would accentuate the features of each profile. The increasing particulate pCo:pP ratio with depth (Fig. 3b) and correlation between pCo and pMn in mesopelagic particles (Fig. 3c, d) indicate that any form of preferential Co remineralization, at least, is overshadowed by a larger return of cobalt to the particulate phase by scavenging (Fig. 3b).

The integrated mesopelagic scavenging flux sums to 0.62 μmol m^{-2} $year^{-1}$ in the South Pacific and 1.36 μmol m^{-2} $year^{-1}$ in the North Atlantic (Fig. 8). There is an additional scavenging flux due to parametrized PO_4 remineralization below 1500 m that does not seem to lead to increased dCo concentrations in the deep ocean (Fig. 2). If this flux is remineralized in a similar stoichiometry as overlying waters (that is, $dCo:PO_{4,remin}$), it would add 0.1 and 0.06 μmol m^{-2} $year^{-1}$ to the areal scavenging flux in the North Atlantic and South Pacific, respectively. This excess scavenging flux does not necessarily occur in the deep ocean if degradation of pCo and pP is sufficiently decoupled (that is, if $pCo:pP_{export}$ decreases with depth).

In both basins, > 50% of the mesopelagic scavenging flux appears to be generated in the upper 500 m. Given the uncertainties associated with determining $pCo:pP_{export}$, the magnitude of the mesopelagic scavenging fluxes should be interpreted with caution. As the range in biogenic pCo:pP values above X_0 is larger than the range below X_0 (hence the log-normal distribution, Fig. 6), and because Ti-correction can sometimes be overzealous (Rauschenberg and Twining, 2015), our calculations may underestimate the cobalt scavenging flux. For instance, if the mean biogenic pCo:pP ratio is used for $pCo:pP_{export}$ instead of the histogram center X_0 (Table 5), resultant scavenging fluxes increase to 1.3 and 3.3 μmol m^{-2} $year^{-1}$ in the South Pacific and North Atlantic, respectively. Still, it is encouraging that our calculations are similar to authigenic Co fluxes to deep ocean sediments in Table 1 (0.3–2.5 μmol m^{-2} $year^{-1}$), especially given the extremely low rates of apparent dCo scavenging in deeper waters (0.09 μmol m^{-2} $year^{-1}$, Fig. 2). This independent calculation also lends cautious support to the assertion that Co accumulation rates in Pacific Ocean sediments have increased since the Pliocene (Kyte et al., 1993).

The areal water column scavenging rate in the North Atlantic is also consistent with higher Co accumulation rates in the Atlantic relative to the Pacific (Table 1) and with multiyear averages from deep sediment traps in the Sargasso Sea (Huang and Conte, 2009). Higher scavenging rates in the Atlantic may be driven by a number of oceanographic factors such as greater biological cobalt utilization in the North Atlantic, or by more extensive cobalt complexation in the Pacific (Hawco et al., 2016; Noble et al., 2012; Saito et al., In Review). Future process and modelling studies should examine the relationship between Co speciation, export, and scavenging to clarify these mechanisms.

The depth distribution of the turnover time of cobalt with respect to scavenging can also be calculated from isopycnal scavenging rates and median dCo concentrations on those isopycnal surfaces (Fig. 9). Both basins show an increasing residence time of dissolved cobalt with depth that approaches the 1000 year turnover time inferred by correlation with deep ocean $\Delta^{14}C$ (Fig. 2). At the very least, the cobalt cycle described herein is internally consistent. The ~50 year residence time of dissolved cobalt in the upper ocean is surprisingly short, but necessary in order to reconcile bulk ocean residence time of 130 years with millennial turnover of cobalt in the deep ocean. Between 100 and 500 m, the slightly higher turnover times in the South Pacific are probably linked to more extensive complexation of dCo as well as dCo storage in the OMZ, where Mn scavenging is inhibited. We also calculate a residence time of cobalt in the surface ocean (0–100 m) based on integrated values of biogenic cobalt export (Table 4) and median dCo values shallower than the isopycnal range used to define the mesopelagic In both the North Atlantic and South Pacific Oceans, surface residence times with respect to biological export are ~1 year, consistent with previous estimations (Saito and Moffett, 2002). Short residence times of cobalt in the euphotic zone and mesopelagic (Fig. 9) suggest that inventories of this metal might be dynamic on short timescales, which may affect the supply of cobalt to the euphotic zone and the extent to which it can be utilized by phytoplankton as a nutrient.

3.5. Sources of cobalt to the ocean

Under steady-state, scavenging removal rates must be balanced by input of new Co to the ocean. The magnitude of these sources is therefore a crucial check on the validity of the water column calculations described above, which indicate a global cobalt sink in marine sediments on the order of 450 Mmol Co per year (Table 6). High resolution datasets from the GEOTRACES era have identified myriad oceanic Co sources: including rivers, continental margins, reducing sediments, dust and hydrothermal vents. Our best attempt to evaluate all of these simultaneously is shown in Table 6. While these calculations are far from definitive, they emphasize the major role of reducing sediments bordering oxygen minimum zones in delivering ~25% of Co to the ocean.

Evidence of a freshwater Co source is readily seen in the western Atlantic, where Gulf Stream waters are enriched to ~100 pM and present strong linear relationships with salinity (Dulaquais et al., 2014a; Saito and Moffett, 2002). Yet, calculating this source is not necessarily straightforward due to desorption of cobalt from terrigenous sediments across salinity gradients and complex redox cycles of Mn and Co in estuarine water columns and sediments (Bewers and Yeats, 1977; Moffett and Ho, 1996; Sunda and Huntsman, 1987). When scaled to the entire ocean, mass balance estimates from the St. Lawrence estuary imply a global cobalt source from these processes of 420 Mmol per year (Bewers and Yeats, 1977). Notably, this is much less than the flux of crustal cobalt delivered to the coastal ocean by fluvial sediments every year (1.8×10^{16} g $year^{-1}$ × 2.9×10^{-7} mol Co g^{-1} upper continental crust = 5200 Mmol per year). Therefore, only ~8% (420 ÷ 5200) of the cobalt delivered to the continental margin by fluvial sources actually makes it to the open ocean. The vast majority is

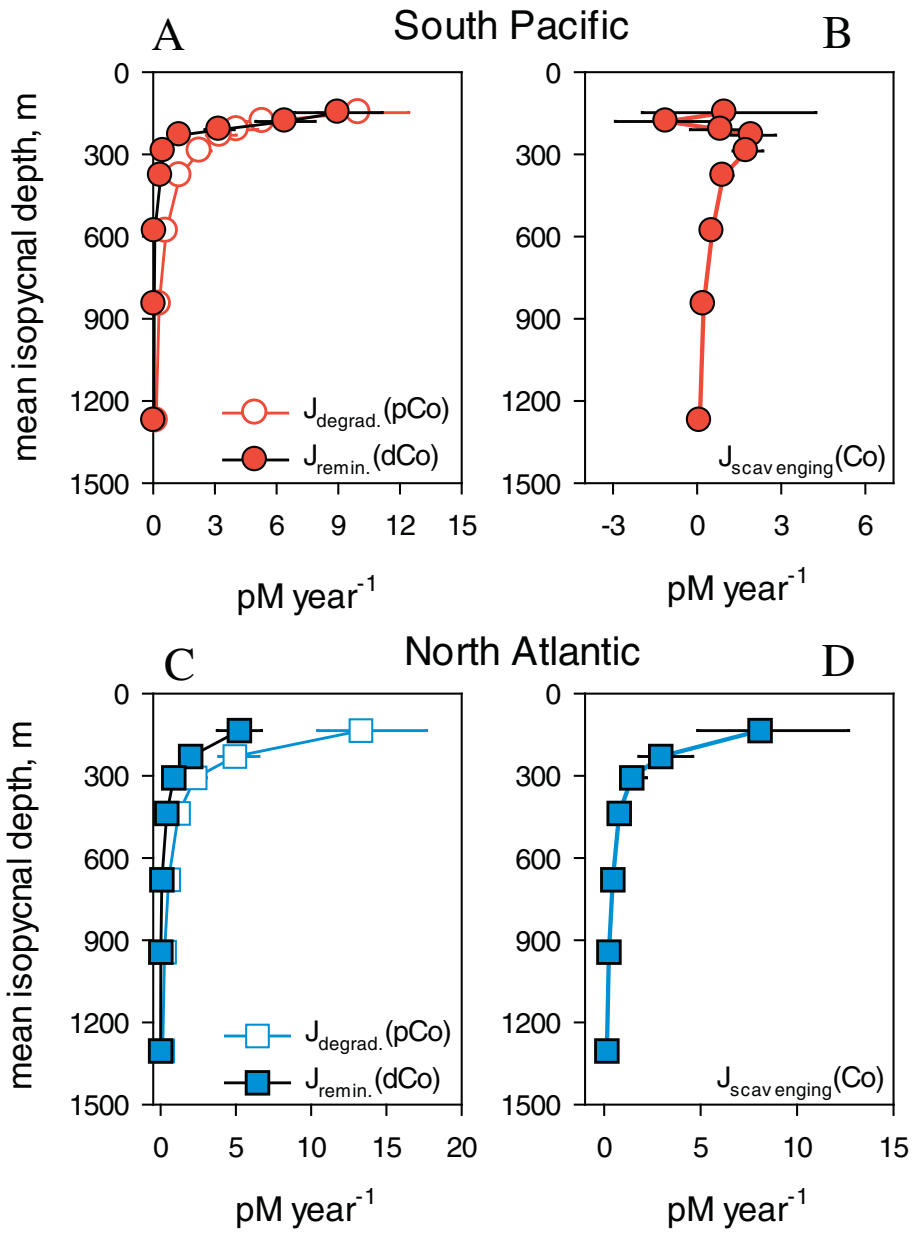

Fig. 7. Mesopelagic cobalt scavenging in the South Pacific (A, B) and North Atlantic (C, D). A, C) particulate Co degradation rates (open squares, from Eq. (7)) and dissolved Co remineralization rates (blue squares, Eq. (5)). C, D) dCo scavenging rates, calculated as the difference between pCo degradation and dCo remineralization rates. Volumetric rates in C, D are calculated from areal rates in Table 4 by dividing by the height of each isopycnal box. (For interpretation of the references to colour in this figure legend, the reader is referred to the web version of this article.)

buried in estuaries and on the continental shelf.

Because almost 55% of fluvial sediments are deposited into marginal seas in Southeast and East Asia, the accuracy of this extrapolation largely depends on the behavior of cobalt in these regions (Milliman and Farnsworth, 2011; Peucker-Ehrenbrink, 2009). A Holocene record of sedimentary Co accumulation in the South China Sea shows Co:Ti ratios ($3.12 \pm 0.24 \times 10^{-3}$ M M^{-1}) that are slightly less than upper continental crust (3.37×10^{-3} M M^{-1}) (Hu et al., 2012; McLennan, 2001), suggesting that about 7% of crustal cobalt delivered to these margins is transported to the open ocean, similar to the value of 8% estimated by extrapolation of the Bewers and Yeats (1977) estimate. However, slow exchange with Pacific Ocean waters and/or elevated rates of Mn-oxidation may cause much of the cobalt released from Southeast and East Asian estuaries to be scavenged before reaching the open ocean.

In contrast, eastern margin sediments underlying OMZs are strongly depleted in cobalt (Böning et al., 2004), implying that the release of cobalt from terrigenous sediments in these areas is more efficient than in oxygenated settings. These observations are corroborated by large plumes of dissolved cobalt in the Atlantic and Pacific OMZs (Hawco et al., 2016; Noble et al., 2017, 2012). Reductive dissolution of Mn-oxides on the margin probably amplifies coastal cobalt sources, resulting in less cobalt buried on the continental margin and a greater source to the open ocean. Indeed, the very low Co:Ti ratios underlying the Peru OMZ ($1.96 \pm 0.55 \times 10^{-3}$ M M^{-1}) relative to crust (3.37×10^{-3} M M^{-1}) imply that 40% of the crustal cobalt delivered to the margin by fluvial sediments is exported to the ocean (Böning et al., 2004). Scaling this observation to include fluvial delivery to the major OMZs in the Atlantic, Pacific, and Indian Oceans implies that, of the 480 Mmol of crustal Co delivered to these regions every year by fluvial sediments (Milliman and Farnsworth, 2011), 200 Mmol Co is released to the open ocean. If these OMZ regions behaved like oxygenated margins such as the St. Lawrence estuary or South China Sea, this source would only be ~40 Mmol cobalt per year. The implication of these calculations is that that deoxygenated coastlines stimulate an additional release of Co to the oceans on the order of 160 Mmol Co · year^{-1}.

Other sources are small. We calculate a dust source integrated from atmospheric deposition models (Jickells et al., 2005) and Co abundance in upper continental crust. Assuming a general 10% solubility

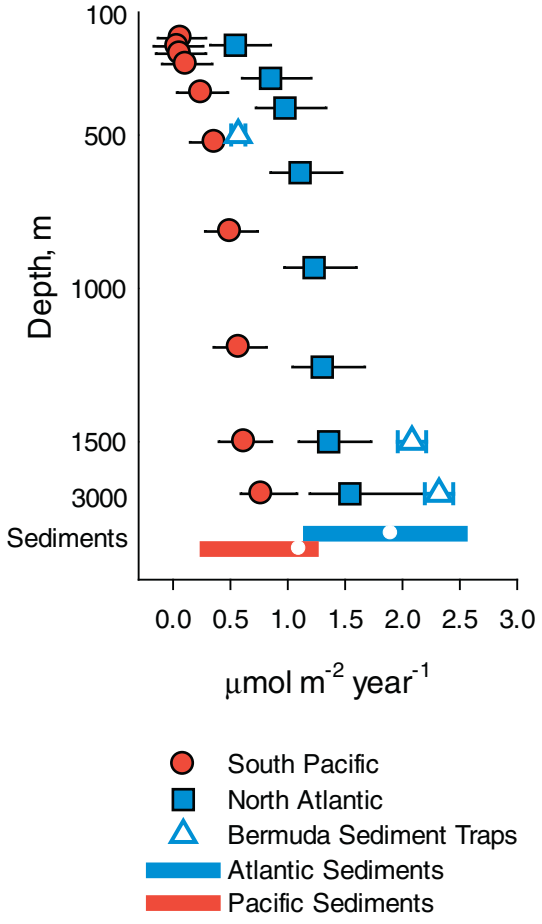

Fig. 8. Integrated cobalt scavenging rates in the North Atlantic (blue squares) and the South Pacific (red circles). The value at each depth represents the contribution from that isopycnal surface and the sum of all overlying isopycnals, akin to what would be collected in a sediment trap. These rates are similar to multiyear averages of Ti-corrected sediments traps from Bermuda (triangles) and excess Co accumulation rates in marine sediments for the Pacific (red line) and Atlantic (blue line); white circles show most likely flux based on the average of Quaternary sediments from Table 1. (For interpretation of the references to colour in this figure legend, the reader is referred to the web version of this article.)

determined from in situ leaching of Saharan dust (Shelley et al., 2012), dust supplies ~12 Mmol Co year^{-1}. Even in the dust-heavy North Atlantic, deposition is < 10% of the Co supplied to the basin. Estimates for a hydrothermal Co flux are also small: ~2 Mmol year^{-1} (Swanner et al., 2014) – even without consideration of rapid near-field scavenging that scrubs ocean sections of any visual evidence of far-field hydrothermal impact (German et al., 1991; Hawco et al., 2016; Noble et al., 2012). Together, atmospheric and hydrothermal input is < 5% of the global source as outlined here.

In sum, our reckoning of global cobalt sources (594 Mmol year^{-1}, Table 6) is sufficient to account for water column scavenging rates (306 Mmol year^{-1}) and the accumulation in pelagic sediments (450 Mmol year^{-1}). Basin-scale budgets for the North Atlantic and South Pacific Oceans composed from regional sums of dust deposition and fluvial sediment delivery show strong agreement as well (Table 3; Jickells et al., 2005; Milliman and Farnsworth, 2011). The comparable magnitudes of cobalt sources and sinks at basin and global scales suggest that the modern cobalt cycle is approximately in balance, at least within the present uncertainties of these calculations.

3.6. A dynamic or stable cobalt cycle?

The high contribution of low-oxygen regions to global cobalt sources (~25%) is surprising and suggests that the supply of cobalt to the ocean may vary synchronously with these oceanographic features. Centennial-scale fluctuations in the volume of anoxic waters associated with modern OMZs in the Pacific have been reported and linked to increased trade wind intensity, which invigorates eastern-boundary upwelling, biological export, and mesopelagic oxygen consumption (Deutsch et al., 2014). Furthermore, anthropogenic warming and stratification appear to limit oxygen resupply from gas exchange on isopycnal outcrops, leading to a decline in mesopelagic O_2 concentrations that is expected to continue over the next century (Stramma et al., 2008). Given the 50–100 year residence time of cobalt in the upper ocean, sustained expansion of OMZs may lead to substantial increases

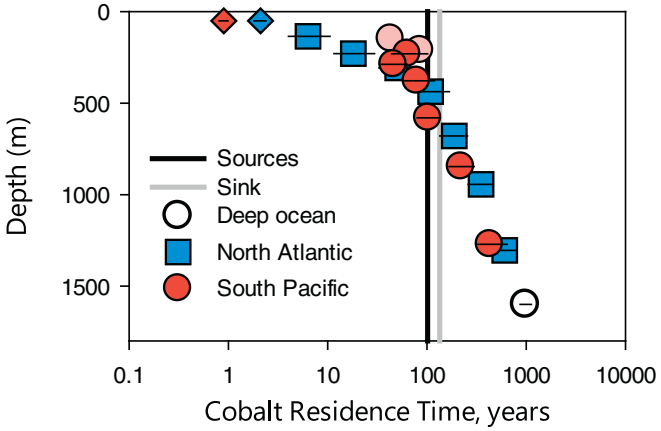

Fig. 9. The residence times of dissolved cobalt in the ocean. Scavenging residence times of cobalt on isopycnal surfaces in the South Pacific (red circles) and North Atlantic (blue squares) are calculated from median dissolved Co concentrations on isopycnal surfaces, divided by water column scavenging rates from Fig. 8B and D, and plotted against the mean depth of the isopycnal window. Pink circles show suggested isopycnal residence times when the scavenging rate was not statistically different from 0. Increasing residence time with depth for both basins intercepts the residence time of deep ocean cobalt, determined by correlation with radiocarbon age (white circle). Bulk residence times by sources (100 years) and Quaternary sediment accumulation rates (130 years) are plotted as black and grey lines, respectively. The residence time of dissolved cobalt in the surface ocean (0–100 m) relative to biological export is plotted as diamonds. (For interpretation of the references to colour in this figure legend, the reader is referred to the web version of this article.)

Table 6
Balance sheet for the marine cobalt cycle. Sums are represented in bold.

Global ($\times 10^6$ mol year^{-1})		Regional (μmol m^{-2} year^{-1})	
		North Atlantic	South Pacific
Sources			
Rivers/estuaries[a]	420	1.41	0.25
OMZs[b]	160	0.65	0.38
Dust[c]	12	0.13	0.01
Hydrothermal[d]	2		
Sum	**594**	**2.19**	**0.64**
Sinks			
Upper Ocean	273 (221–430)	1.46 (1.10–2.11)	0.68 (0.50–0.98)
Deep Ocean	33 (31–35)	0.09 (0.09–0.10)	0.09 (0.09–0.10)
Sum	**306** (252–465)	**1.54** (1.19–2.21)	**0.77** (0.59–1.08)
Sediments[e]	**450** (120-850)	**1.9** (1.2–2.5)	**1.1** (0.3–1.2)

[a] Bewers and Yeats (1977), includes dissolved and particulate sources. Regional scaling based on fluvial sediment delivery maps in Milliman and Farnsworth (2011).
[b] Assumes 40% release of cobalt in sediments deposited on low oxygen coastlines in the Arabian Sea, West Africa, and the western coasts of Mexico, Central America and Northern South America, equal to 1.66 × 10^3 MT year^{-1} (Milliman and Farnsworth, 2011). See text.
[c] Based on 9.3% solubility (Shelley et al., 2012) and dust deposition maps of Jickells et al. (2005).
[d] Swanner et al. 2014.
[e] Values reflect averages of cobalt accumulation rates (K) in Quaternary sediments. Ranges reflect that for all sediments in Table 1.

in oceanic cobalt inventories by exposing a larger swath of coastline to anoxic bottom waters (Noble et al., 2012). Similarly, the apparent contraction of OMZs during glacial periods, suggested by nitrogen isotope and trace metal records (Ganeshram et al., 2000; Jaccard and Galbraith, 2011), may have led to increased burial of cobalt on continental margins by exposing formerly anoxic sediments to oxygen. Hypothesized lower cobalt sources during this time may have affected phytoplankton that depend on this micronutrient for growth (Saito et al., 2002; Sunda and Huntsman, 1995).

This dynamic view of cobalt biogeochemistry, however, is counter to the well-documented steadiness of cobalt accumulation in marine sediments (Dunlea et al., 2015; Kadko, 1985; Krishnaswami, 1976). Since such measurements integrate over dozens, if not hundreds, of revolutions of this cycle, large changes in marine cobalt inventories on 100–1000 year timescales are not inconsistent with these sedimentary observations, provided the existence of stabilizing mechanisms that keep the long-term mean steady. Such mechanisms have been observed on inter-annual timescales, at least. For instance, positive phases of the El Niño Southern Oscillation oxygenate the Peru shelf and have been linked to an increased flux of Mn-oxides to sediments, while negative phases (La Niña) increase anoxia and stimulate dissolution and mobilization of Mn-oxides buried during El Niño years (Scholz et al., 2011). The similarity between Mn and Co cycling in coastal zones implies that cobalt shares a similar fate (Böning et al., 2004). If long-term contraction of OMZs (such as during glacial times) leads to the burial of reactive cobalt in Mn-oxide phases on the margin, this storage may reverse as OMZs expand and Mn-oxides dissolve (e.g. during deglaciation). Analogously, co-precipitation of cobalt during pyrite formation will also decrease the efficiency of anoxic cobalt sources if OMZs intensify to the point that water column sulfate reduction becomes widespread (Morse and Luther, 1999; Scholz et al., 2014). Therefore, there are plausible mechanisms that may stabilize cobalt sources, despite known variability of OMZs on long timescales.

The compilation of modern sources also lends support to the assertion that rates of cobalt accumulation in deep sea sediments of the Pacific are 2–3 times higher during the Quaternary than other times in the Cenozoic (Kyte et al., 1993). Consideration of OMZ sources alone is not enough to explain this change, even though there is some evidence from N-isotope records that OMZs have expanded since the Pliocene (Robinson et al., 2014). Therefore, the increase in cobalt supply requires an increase in riverine/estuarine sources as well. Increased rates of chemical weathering since the Pliocene has been inferred from various isotope systems, and a parallel increase in the chemical weathering of cobalt could explain the shift to higher cobalt accumulation rates in sediments, but this remains controversial (Willenbring and von Blanckenburg, 2010). More thorough investigations into cobalt accumulation rates in marine sediments would lend greater confidence in these assertions.

4. Conclusions

In addition to biological cycling, dissolved cobalt concentrations in seawater are impacted by scavenging. The excess cobalt in marine sediments provides a record of the magnitude of the water column scavenging flux. Correlations between dissolved cobalt and radiocarbon age indicate that scavenging rates in the deep ocean are low while indirect calculations of cobalt scavenging in the mesopelagic can account for most of the cobalt flux to marine sediments. High rates of scavenging in the mesopelagic and slower scavenging in the deep ocean generate a bi-modal distribution of oceanic residence times. Extraordinarily long-lived cobalt in the deep ocean has a turnover time of ~1000 years, while cobalt travels from source to sink in the upper ocean in a matter of decades. These fast and slow lanes of the cobalt cycle average to a mean residence time of 130 years.

Scavenging sinks are balanced by cobalt sources to the ocean and about 25% of cobalt sources may stem from low-oxygen regions on eastern margins, where burial of cobalt in Mn-oxide phases is unfavorable. Despite its reputation as a 'constant' flux recorder in pelagic sediments and ferromanganese nodules and crusts, it seems not only possible but likely for climate-driven changes in oceanic OMZs to have a strong effect on the amount of cobalt supplied to the ocean. In addition to its role as a nutrient to phytoplankton, the potential for cobalt inventories to change with ocean oxygenation may be a useful paleoceanographic tool for constraining the variability of OMZs in past climates.

Author contributions

NJH, AEN, NJW, MCL and MAS measured and interpreted dissolved cobalt on the GP16, GA03, GAc01, GPc3 and GA10 cruises. JML, DCO and PJL measured and interpreted particulate trace elements on the GP16 and GA03 cruises. This manuscript was written by NJH and MAS with contributions from all authors.

Acknowledgements

We thank Ann Dunlea, Tristan Horner, and Mick Follows for helpful discussions as well as the GA03 and GP16 sampling teams that collected these data. The GEOTRACES office provided funding for data workshops that facilitated this synthesis. This work was funded by National Science Foundation Grants OCE-1233261, 0928414, 0963026, 1518110, NERC grant NE/H004475/1 and the Gordon Betty Moore Foundation (Grant 3738).

Appendix A. Supplementary data

Supplementary data to this article can be found online at http://dx.doi.org/10.1016/j.marchem.2017.09.001.

References

Bacon, M.P., Rosholt, J.N., 1982. Accumulation rates of Th-230, Pa-231, and some transition metals on the Bermuda Rise. Geochimica et Cosmochimica Acta 46 (4), 651–666.

Bewers, J.M., Yeats, P.A., 1977. Oceanic residence times of trace metals. Nature 268, 595–598.

Böning, P., Brumsack, H.-J., Böttcher, M.E., Schnetger, B., Kriete, C., Kallmeyer, J., Borchers, S.L., 2004. Geochemistry of Peruvian near-surface sediments. Geochim. Cosmochim. Acta 68, 4429–4451. http://dx.doi.org/10.1016/j.gca.2004.04.027.

Bown, J., Boye, M., Baker, A., Duvieilbourg, E., Lacan, F., Le Moigne, F., Planchon, F., Speich, S., Nelson, D.M., 2011. The biogeochemical cycle of dissolved cobalt in the Atlantic and the Southern Ocean south off the coast of South Africa. Mar. Chem. 126, 193–206. http://dx.doi.org/10.1016/j.marchem.2011.03.008.

Broecker, W.S., Blanton, S., Smethie, W.M., 1991. Radiocarbon decay and oxygen utilization in the deep atlantic ocean. Glob. Biogeochem. Cycles 5.

Cowen, J.P., Bruland, K.W., 1985. Metal deposits associated with bacteria: implications for Fe and Mn marine biogeochemistry. Deep Sea Res. Part A. Oceanogr. Res. Pap. 32, 253–272. http://dx.doi.org/10.1016/0198-0149(85)90078-0.

Deutsch, C., Berelson, W., Thunell, R., Weber, T., Tems, C., McManus, J., Crusius, J., Ito, T., Baumgartner, T., Ferreira, V., Mey, J., van Geen, A., 2014. Centennial changes in North Pacific anoxia linked to tropical trade winds. Science 345, 665–668. http://dx.doi.org/10.1126/science.1252332.

D'Hondt, S., Inagaki, F., Zarikian, C.A., Abrams, L.J., Dubois, N., Engelhardt, T., Evans, H., Ferdelman, T., Gribsholt, B., Harris, R.N., Hoppie, B.W., Hyun, J.-H., Kallmeyer, J., Kim, J., Lynch, J.E., McKinley, C.C., Mitsunobu, S., Morono, Y., Murray, R.W., Pockalny, R., Sauvage, J., Shimono, T., Shiraishi, F., Smith, D.C., Smith-Duque, C.E., Spivack, A.J., Steinsbu, B.O., Suzuki, Y., Szpak, M., Toffin, L., Uramoto, G., Yamaguchi, Y.T., Zhang, G., Zhang, X.-H., Ziebis, W., 2015. Presence of oxygen and aerobic communities from sea floor to basement in deep-sea sediments. Nat. Geosci. 8, 299–304. http://dx.doi.org/10.1038/ngeo2387.

Dulaquais, G., Boye, M., Middag, R., Owens, S., Puigcorbe, V., Buesseler, K., Masqué, P., de Baar, H.J.W., Carton, X., 2014a. Contrasting biogeochemical cycles of cobalt in the surface western Atlantic Ocean. Glob. Biogeochem. Cycles 28, 1387–1412. http://dx.doi.org/10.1002/2014GB004903.

Dulaquais, G., Boye, M., Rijkenberg, M.J. a, Carton, X., 2014b. Physical and remineralization processes govern the cobalt distribution in the deep western Atlantic Ocean. Biogeosciences 11, 1561–1580. http://dx.doi.org/10.5194/bg-11-1561-2014.

Dunlea, A.G., Murray, R.W., Harris, R.N., 2015. Cobalt-based age models of pelagic clay in the South Pacific Gyre. Geochem. Geophys. Geosys. 16 (8), 2694–2710.

Eakins, B.W., Sharman, G.F., 2010. Volumes of the World's Oceans from ETOPO1. NOAA Natl. Geophys. Data Center, Boulder, CO.

Fiedler, P.C., Talley, L.D., 2006. Hydrography of the eastern tropical Pacific: a review. Prog. Oceanogr. 69, 143–180. http://dx.doi.org/10.1016/j.pocean.2006.03.008.

Frank, M., O'Nions, R.K., Hein, J.R., Banakar, V.K., 1999. 60 Myr records of major elements and Pb-Nd isotopes from hydrogenous ferromanganese crusts: reconstruction of seawater paleochemistry. Geochim. Cosmochim. Acta 63, 1689–1708. http://dx.doi.org/10.1016/S0016-7037(99)00079-4.

Ganeshram, R.S., Pedersen, T.F., Calvert, S.E., McNeill, G.W., Fontugne, M.R., 2000. Glacial-interglacial variability in denitrification in the World's oceans: causes and consequences. Paleoceanography 15, 361–376.

German, C.R., Campbell, A.C., Edmond, J.M., 1991. Hydrothermal scavenging at the Mid-Atlantic Ridge: modification of trace element dissolved fluxes. Earth Planet. Sci. Lett. 107, 101–114. http://dx.doi.org/10.1016/0012-821X(91)90047-L.

Goldberg, E.D., Arrhenius, G.O.S., 1958. Chemistry of Pacific pelagic sediments. Geochim. Cosmochim. Acta 13, 153–212. http://dx.doi.org/10.1016/0016-7037(58)90046-2.

Gouretski, V.V., Koltermann, K.P., 2004. WOCE Global Hydrographic Climatology. 35/2004. Berichte des Bundesamtes fur Seeschifffahrt und Hydrographie, pp. 52.

Halbach, P., Segl, M., Puteanus, D., Mangini, A., 1983. Co-fluxes and growth rates in ferromanganes deposits from central Pacific seamount seas. Nature 304, 716–719.

Hawco, N.J., Ohnemus, D.C., Resing, J.A., Twining, B.S., Saito, M.A., 2016. A cobalt plume in the oxygen minimum zone of the Eastern Tropical South Pacific. Biogeosciences 13, 5697–5717. http://dx.doi.org/10.5194/bg-2016-169.

Heggie, D., Lewis, T., 1984. Cobalt in pore waters of marine sediments. Nature 311 (5985), 453–455.

Hu, D., Böning, P., Köhler, C.M., Hillier, S., Pressling, N., Wan, S., Brumsack, H.J., Clift, P.D., 2012. Deep sea records of the continental weathering and erosion response to East Asian monsoon intensification since 14 ka in the South China Sea. Chem. Geol. 326–327, 1–18. http://dx.doi.org/10.1016/j.chemgeo.2012.07.024.

Huang, S., Conte, M.H., 2009. Source/process apportionment of major and trace elements in sinking particles in the Sargasso sea. Geochim. Cosmochim. Acta 73, 65–90. http://dx.doi.org/10.1016/j.gca.2008.08.023.

Jaccard, S.L., Galbraith, E.D., 2011. Large climate-driven changes of oceanic oxygen concentrations during the last deglaciation. Nat. Geosci. 5, 151–156. http://dx.doi.org/10.1038/ngeo1352.

Jakuba, R.W., Moffett, J.W., Dyhrman, S.T., 2008. Evidence for the linked biogeochemical cycling of zinc, cobalt, and phosphorus in the western North Atlantic Ocean. Glob. Biogeochem. Cycles 22, 1–13. http://dx.doi.org/10.1029/2007GB003119.

Jenkins, W.J., Smethie Jr., W.M., Boyle, E.A., Cutter, G.A., 2014. Water mass analysis for the U.S. GEOTRACES (GA03) North Atlantic sections. Deep Sea Res. Part II Top. Stud. Oceanography 1–30. http://dx.doi.org/10.1016/j.dsr2.2014.11.018.

Jenkins, W.J., Lott, D.E., Longworth, B.E., Curtice, J.M., Cahill, K.L., 2015. The distributions of helium isotopes and tritium along the U.S. GEOTRACES North Atlantic sections (GEOTRACES GAO3). Deep. Res. Part II Top. Stud. Oceanogr. 116, 21–28. http://dx.doi.org/10.1016/j.dsr2.2014.11.017.

Jickells, T.D., An, Z.S., Andersen, K.K., Baker, A.R., Bergametti, G., Brooks, N., Cao, J.J., Boyd, P.W., Duce, R.A., Hunter, K.A., 2005. Global iron connections between desert dust, ocean biogeochemistry, and climate. Science 308, 67–71.

Kadko, D., 1985. Late Cenozoic sedimentation and metal deposition in the North Pacific. Geochim. Cosmochim. Acta 49, 651–661. http://dx.doi.org/10.1016/0016-7037(85)90160-7.

Karstensen, J., Stramma, L., Visbeck, M., 2008. Oxygen minimum zones in the eastern tropical Atlantic and Pacific oceans. Prog. Oceanogr. 77, 331–350. http://dx.doi.org/10.1016/j.pocean.2007.05.009.

Key, R.M., Kozyr, a., Sabine, C.L., Lee, K., Wanninkhof, R., Bullister, J.L., Feely, R.a., Millero, F.J., Mordy, C., Peng, T.H., 2004. A global ocean carbon climatology: results from global data analysis project (GLODAP). Glob. Biogeochem. Cycles 18, 1–23. http://dx.doi.org/10.1029/2004GB002247.

Krishnaswami, S., 1976. Authigenic transition elements in Pacific pelagic clays. Geochim. Cosmochim. Acta 40, 425–434. http://dx.doi.org/10.1016/0016-7037(76)90007-7.

Kyte, F.T., Leinen, M., Ross Heath, G., Zhou, L., 1993. Cenozoic sedimentation history of the central North Pacific: inferences from the elemental geochemistry of core LL44-GPC3. Geochim. Cosmochim. Acta 57, 1719–1740. http://dx.doi.org/10.1016/0016-7037(93)90109-A.

von Langen, P.J., Johnson, K.S., Coale, K.H., Elrod, V.a., 1997. Oxidation kinetics of manganese (II) in seawater at nanomolar concentrations. Geochim. Cosmochim. Acta 61, 4945–4954. http://dx.doi.org/10.1016/S0016-7037(97)00355-4.

Manheim, F.T., 1986. Marine cobalt resources. Science (80-.).

Matsumoto, K., 2007. Radiocarbon-based circulation age of the world oceans. J. Geophys. Res. Ocean. 112, 1–7. http://dx.doi.org/10.1029/2007JC004095.

McLennan, S.M., 2001. Relationships between the trace element composition of sedimentary rocks and upper continental crust. Geochem. Geophys. Geosyst. 2 n/a–n/a. http://dx.doi.org/10.1029/2000GC000109.

Milliman, J.D., Farnsworth, K.L., 2011. River Discharge to the Coastal Ocean, Cambridge University Press. Cambridge University Press, Cambridge. http://dx.doi.org/10.1017/CBO9780511781247.

Moffett, J.W., Ho, J., 1996. Oxidation of cobalt and manganese in seawater via a common microbially catalyzed pathway. Geochim. Cosmochim. Acta 60, 3415–3424. http://dx.doi.org/10.1016/0016-7037(96)00176-7.

Moore, C.M., Mills, M.M., Arrigo, K.R., Berman-Frank, I., Bopp, L., Boyd, P.W., Galbraith, E.D., Geider, R.J., Guieu, C., Jaccard, S.L., Jickells, T.D., La Roche, J., Lenton, T.M., Mahowald, N.M., Marañón, E., Marinov, I., Moore, J.K., Nakatsuka, T., Oschlies, A., Saito, M. a, Thingstad, T.F., Tsuda, A., Ulloa, O., 2013. Processes and patterns of oceanic nutrient limitation. Nat. Geosci. 6, 701–710. http://dx.doi.org/10.1038/ngeo1765.

Morse, J.W., Luther, G.W., 1999. Chemical influence on trace metalsulphide interactions in anoxic sediments. Geochim. Cosmochim. Acta 63, 3378.

Noble, A.E., Lamborg, C.H., Ohnemus, D.C., Lam, P.J., Goepfert, T.J., Measures, C.I., Frame, C.H., Casciotti, K.L., DiTullio, G.R., Jennings, J., Saito, M.A., 2012. Basin-scale inputs of cobalt, iron, and manganese from the Benguela-Angola front to the South Atlantic Ocean. Limnol. Oceanogr. 57, 989–1010. http://dx.doi.org/10.4319/lo.2012.57.4.0989.

Noble, A.E., Ohnemus, D.C., Hawco, N.J., Lam, P.J., Saito, M.A., 2017. Coastal sources, sinks and strong organic complexation of dissolved cobalt within the US North Atlantic GEOTRACES transect GA03. Biogeosciences 14, 2715–2739. http://dx.doi.org/10.5194/bg-14-2715-2017.

Ohnemus, D.C., Lam, P.J., 2015. Cycling of lithogenic marine particles in the US GEOTRACES North Atlantic transect. Deep Sea Res. Part II Top. Stud. Oceanogr. 116, 283–302. http://dx.doi.org/10.1016/j.dsr2.2014.11.019.

Ohnemus, D.C., Rauschenberg, S., Cutter, G.A., Fitzsimmons, J.N., Sherrell, R.M., Twining, B.S., 2016. Elevated trace metal content of prokaryotic plankton communities associated with marine oxygen deficient zones. Limnol. Oceanogr Accepted. http://dx.doi.org/10.1002/lno.10363.

Peucker-Ehrenbrink, B., 2009. Land2Sea database of river drainage basin sizes, annual water discharges, and suspended sediment fluxes. Geochem. Geophys. Geosyst. 10, 1–10. http://dx.doi.org/10.1029/2008GC002356.

Rauschenberg, S., Twining, B.S., 2015. Evaluation of approaches to estimate biogenic particulate trace metals in the ocean. Mar. Chem. 171, 67–77. http://dx.doi.org/10.1016/j.marchem.2015.01.004.

Robinson, R.S., Etourneau, J., Martinez, P.M., Schneider, R., 2014. Expansion of pelagic denitrification during early Pleistocene cooling. Earth Planet. Sci. Lett. 389, 52–61. http://dx.doi.org/10.1016/j.epsl.2013.12.022.

Saito, M.A., Moffett, J.W., 2001. Complexation of cobalt by natural organic ligands in the Sargasso Sea as determined by a new high-sensitivity electrochemical cobalt speciation method suitable for open ocean work. Mar. Chem. 75, 49–68. http://dx.doi.org/10.1016/S0304-4203(01)00025-1.

Saito, M.A., Moffett, J.W., 2002. Temporal and spatial variability of cobalt in the Atlantic Ocean. Geochim. Cosmochim. Acta 66, 1943–1953. http://dx.doi.org/10.1016/S0016-7037(02)00829-3.

Saito, M.A., Moffett, J.W., Chisholm, S.W., Waterbury, J.B., 2002. Cobalt limitation and uptake in prochlorococcus. Limnol. Oceanogr. 47, 1629–1636. http://dx.doi.org/10.4319/lo.2002.47.6.1629.

Saito, M.A., Moffett, J.W., DiTullio, G.R., 2004. Cobalt and nickel in the Peru upwelling region: a major flux of labile cobalt utilized as a micronutrient. Glob. Biogeochem. Cycles 18 (n/a–n/a). http://dx.doi.org/10.1029/2003GB002216.

Saito, M.A., Rocap, G., Moffett, J.W., 2005. Production of cobalt binding ligands in a Synechococcus feature at the Costa Rica upwelling dome. Limnol. Oceanogr. 50, 279–290. http://dx.doi.org/10.4319/lo.2005.50.1.0279.

Saito, M.A., Goepfert, T.J., Noble, A.E., Bertrand, E.M., Sedwick, P.N., DiTullio, G.R., 2010. A seasonal study of dissolved cobalt in the Ross Sea, Antarctica: micronutrient behavior, absence of scavenging, and relationships with Zn, Cd, and P. Biogeosciences 7, 4059–4082. http://dx.doi.org/10.5194/bg-7-4059-2010.

Saito et al., In Review, Accepted https://doi.org/10.5194/bg-2016-511.

Sañudo-Wilhelmy, S.A., Olsen, K.A., Scelfo, J.M., Foster, T.D., Flegal, A.R., 2002. Trace metal distributions off the antarctic peninsula in the weddell sea. Mar. Chem. 77, 157–170. http://dx.doi.org/10.1016/S0304-4203(01)00084-6.

Scholz, F., Hensen, C., Noffke, A., Rohde, A., Liebetrau, V., Wallmann, K., 2011. Early diagenesis of redox-sensitive trace metals in the Peru upwelling area - response to ENSO-related oxygen fluctuations in the water column. Geochim. Cosmochim. Acta 75, 7257–7276. http://dx.doi.org/10.1016/j.gca.2011.08.007.

Scholz, F., McManus, J., Mix, A.C., Hensen, C., Schneider, R.R., 2014. The impact of ocean deoxygenation on iron release from continental margin sediments. Nat. Geosci. 7, 433–437. http://dx.doi.org/10.1038/ngeo2162.

Shaked, Y., Xu, Y., Leblanc, K., Morel, F.M.M., 2006. Zinc availability and alkaline phosphatase activity in Emiliania huxleyi: implications for Zn-P co-limitation in the ocean. Limnol. Oceanogr. 51, 299–309. http://dx.doi.org/10.4319/lo.2006.51.1.0299.

Shelley, R.U., Sedwick, P.N., Bibby, T.S., Cabedo-Sanz, P., Church, T.M., Johnson, R.J., Macey, A.I., Marsay, C.M., Sholkovitz, E.R., Ussher, S.J., Worsfold, P.J., Lohan, M.C., 2012. Controls on dissolved cobalt in surface waters of the Sargasso Sea: comparisons with iron and aluminum. Glob. Biogeochem. Cycles 26 n/a–n/a. http://dx.doi.org/10.1029/2011GB004155.

Shelley, R.U., Morton, P.L., Landing, W.M., 2015. Elemental ratios and enrichment factors in aerosols from the US-GEOTRACES North Atlantic transects. Deep. Res. Part II Top. Stud. Oceanogr. 116, 262–272. http://dx.doi.org/10.1016/j.dsr2.2014.12.005.

Stramma, L., Johnson, G.C., Sprintall, J., Mohrholz, V., 2008. Expanding oxygen-minimum zones in the tropical oceans. Science 320, 655–658. http://dx.doi.org/10.1126/science.1153847.

Sunda, W.G., Huntsman, S.A., 1987. Microbial oxidation of manganese in a North Carolina estuary. Limnol. Oceanogr. 32, 552–564. http://dx.doi.org/10.4319/lo.1987.32.3.0552.

Sunda, W.G., Huntsman, S.A., 1988. Effect of sunlight on redox cycles of manganese in the southwestern Sargasso Sea. Deep Sea Res. Part A. Oceanogr. Res. Pap. 35, 1297–1317. http://dx.doi.org/10.1016/0198-0149(88)90084-2.

Sunda, W.G., Huntsman, S.A., 1990. Diel cycles in microbial manganese oxidation and manganese redox speciation in coastal waters of the Bahama Islands. Limnol. Oceanogr. 35, 325–338. http://dx.doi.org/10.4319/lo.1990.35.2.0325.

Sunda, W.G., Huntsman, S.A., 1995. Cobalt and zinc interreplacement in marine phytoplankton: biological and geochemical implications. Limnol. Oceanogr. 40, 1404–1417. http://dx.doi.org/10.4319/lo.1995.40.8.1404.

Swanner, E.D., Planavsky, N.J., Lalonde, S.V., Robbins, L.J., Bekker, A., Rouxel, O.J., Saito, M.A., Kappler, A., Mojzsis, S.J., Konhauser, K.O., 2014. Cobalt and marine redox evolution. Earth Planet. Sci. Lett. 390, 253–263. http://dx.doi.org/10.1016/j.

epsl.2014.01.001.

Teng, Y., Primeau, F.W., Moore, J.K., Lomas, M.W., Martiny, A.C., 2014. Global-scale variations of the ratios of carbon to phosphorus in exported marine organic matter. Nat. Geosci. 7, 2–5. http://dx.doi.org/10.1038/NGEO2303.

Thomson, J., et al., 1984. Metal accumulation rates in Northwest Atlantic pelagic sediments. Geochimica et Cosmochimica Acta 48 (10), 1935–1948.

Tovar-Sánchez, A., Sañudo-Wilhelmy, S.A., Flegal, A.R., 2004. Temporal and spatial variations in the biogeochemical cycling of cobalt in two urban estuaries: Hudson River Estuary and San Francisco Bay. Estuar. Coast. Shelf Sci. 60, 717–728. http://dx.doi.org/10.1016/j.ecss.2004.03.010.

Turekian, K.K., 1968. Deep-sea deposition of barium, cobalt and silver. Geochimica et Cosmochimica Acta 32 (6), 603–612.

Willenbring, J.K., von Blanckenburg, F., 2010. Long-term stability of global erosion rates and weathering during late-Cenozoic cooling. Nature 465, 211–214. http://dx.doi.org/10.1038/nature09044.

Windom, H.L., 1970. Contribution of atmospherically transported trace metals to South Pacific sediments. Geochimica et cosmochimica acta 34 (4), 509–514.

Xu, Y., Tang, D., Shaked, Y., Morel, F.M.M., 2007. Zinc, cadmium, and cobalt interreplacement and relative use efficiencies in the coccolithophore Emiliania huxleyi. Limnol. Oceanogr. 52, 2294–2305. http://dx.doi.org/10.4319/lo.2007.52.5.2294.

Yee, D., Morel, F.M.M., 1996. In vivo substitution of zinc by cobalt in carbonic anhydrase of a marine diatom. Limnol. Oceanogr. 41, 573–577. http://dx.doi.org/10.4319/lo.1996.41.3.0573.

Zhang, Y., Rodionov, D.A., Gelfand, M.S., Gladyshev, V.N., 2009. Comparative genomic analyses of nickel, cobalt and vitamin B12 utilization. BMC Genomics 10, 78. http://dx.doi.org/10.1186/1471-2164-10-78.

Zhou, L., Kyte, F.T., 1992. Sedimentation history of the south pacific pelagic clay province over the last 85 million years inferred from the geochemistry of deep sea drilling project hole 596. Paleoceanography 7, 441–465.